University of Warsaw
Faculty of Physics

Maciej Łebek
Record book number 370367

Elementary excitations of one-dimensional dipolar quantum Bose droplets

Master's thesis
in the field of Physics (studies in English)

The thesis was written under the supervision of
dr hab. Krzysztof Pawłowski
Center for Theoretical Physics PAS
dr hab. Jan Chwedeńczuk
Chair of Quantum Optics and Atomic Physics
Institute of Theoretical Physics

Warsaw, September 2021

Summary

One-dimensional bosonic gas with attractive dipolar and strong short-range repulsive interactions features the so-called quantum droplets. Quantum droplets are ultradilute analogues of classical droplets that are stabilized by quantum fluctuations. In this thesis, we propose a simple hydrodynamic theory of one-dimensional bosonic dipolar gas. The introduced theory is build with the information taken from the integrable Lieb-Liniger (LL) model and is formulated in a form of mean-field equation called here the Lieb-Liniger-Gross-Pitaevskii (LLGP) equation. We classify the phases visible in our model and derive analytical approximations valid in certain regimes. The main goal of the thesis is to study elementary excitations. In the absence of dipolar interactions, we directly compare predicitions of our model with the exact results from the LL model, obtaining good agreement. After these initial tests, we move to the case of excitations displayed by a quantum droplet. We obtain shapes of collective modes and excitation energies as a solutions of Bogoliubov-de Gennes equations. These numerical results are supplemented by analytical approximations.

Keywords

quantum gas, bosons, quantum droplets, mean-field theory

Title of the thesis in Polish language

Wzbudzenia elementarne jednowymiarowych, bozonowych kropli kwantowych z oddziaływaniami dipolowymi.

Contents

Chapter 1

Introduction

The subject of the thesis is embedded in a context of research related to ultracold atomic physics. Experimental advances of the recent decades opened a way to explore properties of gases at very low temperatures, where the atoms move so slowly that their behavior is essentially quantum. Due to the very low densities of the atomic clouds, it is possible to reach such regime avoiding crystallization. The resulting phase of matter is called quantum gas. Nowadays, such gases are routinely prepared in the laboratories and astonishing effects such as the Bose-Einstein condensation [1, 2] or interference of matter waves [3], are observed and studied by the experimentalists.

The field of ultracold physics was born with the papers of Bose and Einstein concerning thermodynamical properties of indistinguishable particles. Such particles may be divided into two groups: bosons and fermions. An arbitrary number of bosons can occupy the same quantum state as opposed to fermions for which only one particle per quantum state is allowed. Einstein predicted that a quantum gas consisting of bosonic particles undergoes a phase transition. Below the critical temperature, a macroscopic number of atoms occupy the same quantum state, forming a condensate - a large matter wave that can interfere with other condensates. These predictions motivated experimentalists to reach cool a gas to lower and lower temperatures. Several important experimental techniques concerning cooling and trapping were developed for that purpose. The Nobel prize for some of these inventions were awarded to S. Chu, C. Cohen-Tannoudji and W. Philips in 1997. Four years later, another Nobel prize was given to W. Ketterle, E. Cornell and C. Wieman for the experimental realization of Bose-Einstein condensate [1, 2].

This discovery was a milestone that accelerated both experimental and theoretical studies of quantum gases. Since that time, a plethora of different experiments probed the quantum behavior of ultracold atoms. Moreover, the ultracold gas turned out to be an extremely controllable system. Physicists are able to manipulate interparticle interactions and trap the atoms into potentials of a variety of different geometries. Importantly, thanks to strongly anisotropic confinement, also physics in lower dimensionalities is explored in the laboratories. For example, one-dimensional geometry is effectively obtained when the energy related to the first excited state of a transversal confinement is much bigger than average energies associated with longitudinal degrees of freedom. It is no surprise, that with such a controlable systems at hand, that new, exotic effects are still being discovered.

So it happened in 2015, when the group of T. Pfau discovered a new state of ultracold matter - a dilute quantum droplet [4]. Typically, a quantum gas in its ground state is characterized by an uniform density (with some deviations from that caused by the trapping). On the other hand, quantum droplet phase corresponds to the situation, where the gas breaks

the translational symmetry in its ground state and forms self-bound finite-size droplets. The experiment [4] was performed using a bosonic quantum gas with interactions characterized by repulsive short-range character and a long-range dipolar attraction. Competition between these two forces drives the formation of quantum droplets. A similar type of interaction is also responsible for the stability of classical droplets, although in the quantum case we deal with much lower densities and temperatures.

Around the same time, a theoretical paper by D. Petrov [5] predicted existence of similar ultracold droplets in a different setup involving a mixture of two Bose gases. This time however, the appearence of droplets required a fine-tuning of intra- and interspecies interactions between bosons. Relevant conditions may be understood via energy considerations. In the proposed setup, intracomponent interactions are repulsive, whereas intercomponent interactions are attractive. In such case energy of the uniform gas may be written, using the simplest approximation known as the mean-field approximation, as $E = \frac{1}{2}\delta g n^2$ with $\delta g < 0$ where n is the density of atoms. Therefore, to minimize the energy, the gas should shrink to a point to maximize the local density. Such behaviour is indeed observed experimentally for large $|\delta g|$. Unexpectedly, the situation changes, when the term δg is made very small, for instance by proper tuning of inter- and intra-component couplings. In such a case, Petrov showed that also higher order (beyond mean-field) term in the gas density n has to be taken into account

$$E = \frac{1}{2}\delta g n^2 + C_{\mathrm{LHY}} n^{5/2}. \tag{1.1}$$

The paper [5] points out situation where simultaneously $\delta g < 0$ is small and $C_{\mathrm{LHY}} > 0$. The beyond mean-field term is called Lee-Huang-Yang correction [6] and stems from energy associated with quantum fluctuations. Crucially, the energy (1.1) as a function of density displays a local minimum for a finite value of density. It means that it is energetically favorable to form a state with that specific value of the density. Consecutive studies shown that this state is a new phase of matter, called a quantum droplet. Droplets in two-component Bose gases predicted by Petrov were realized in the experiment in 2018 [7].

In general, one expects quantum droplets in any case, where the energy of the homogenous gas consists of two competing terms that depend in a different way on the density, guaranteeing local minimum for finite density. This may be the case also in setups involving different interactions and lower dimensions [8, 9, 10]. In particular, such form of the energy is visible in one-dimensional, strongly interacting dipolar Bose gas that is studied in this thesis. The paper [11] shown that quantum droplets should exist in the regime of strong, contact repulsion and weak, dipolar attraction. In this case, the energy coming from very strong short range interaction is expressed by $E \sim n^4$, instead of $E_{\mathrm{con}} \sim n^2$ valid for weak interactions. On the other hand, attractive and weak dipolar interactions lead to energy scaling with density as $E_{\mathrm{dip}} \sim n^2$. In the presence of both types of interactions, the total energy given by $E_{\mathrm{con}} + E_{\mathrm{dip}}$, posses a local minimum corresponding to a droplet density.

The thesis is solely dedicated to the one-dimensional dipolar gas featuring droplets introduced in [11]. We introduce a slightly more accurate version of the effective mean-field equation and extend the analysis of the phase diagram with the droplet phase. However, the main goal of the thesis is to study elementary excitations exhibited by the quantum droplets. In other words, we analyze the response of a droplet to small perturbation by identifying shapes of the elementary modes and associated excitation energies. This is done by solution of so-called Bogoliubov-de Gennes (BdG) equations that give modes and excitation energies.

Structure of the thesis

In Chapter 2 we present a brief introduction to the mean-field description of repulsive Bose gases. We start with a derivation and discussion of a well-known Gross-Pitaevskii (GP) equation suitable for weakly interacting and stable gas. This is followed by introduction of hydrodynamical equations constructed with the local energy density taken from the Lieb-Liniger (LL) model. The proposed equations are aimed at the regime of strong interactions and are benchmarked with the exact results for elementary excitations known in the LL model. In Chapter 3 we discuss dipolar interactions in 1D and propose an effective mean-field equation describing gas with strong contact repulsion and long-range dipolar attraction. Such equation may be seen as an extension of the approach introduced and benchmarked in the Chpater 2. We then identify different phases found in the stationary solution of the equation. Among them, we thoroughly describe solutions corresponding to quantum droplets in different regimes of the interactions. Finally, we move to the analysis of elementary excitations in Chapter 4. We solve BdG equations both numerically and analytically characterizing excitations in different regimes. A summary of the obtained results is presented in the last chapter.

Chapter 2

Effective descriptions of a repulsive Bose gas

Throughout this work we deal with a system of N cold bosons confined to 1D geometry. We assume periodic boundary conditions, applicable for instance to a system of atoms placed on a ring of length L. The Hamiltonian governing system of particles interacting via interaction potential $V(x-x')$ takes the following form

$$H = -\frac{\hbar^2}{2m}\sum_{j=1}^{N}\partial_{x_i}^2 + \sum_{i<j} V(x_i - x_j), \tag{2.1}$$

where m denotes mass of the atoms. Diagonalization of such a Hamiltonian when N is large and $V \neq 0$ is possible only for a couple of models for which there exist exact solutions. Arguably the most important one is the LL model [12, 13] of bosons interacting via a contact potential $V(x-x') = g\delta(x-x')$, where g is the coupling constant. However, even in the case of the LL model, the number of involved degrees of freedom is very large. As a result, it is difficult to extract physical information due to the complexity of the many-body eigenstates. Hence, one is forced to replace analytical approach with an effective description of a quantum gas that focuses on some particular observables and regimes of parameters. Such approach inherently leads to a loss of some information about the system (such as the interparticle correlations). Nevertheless, it sets up a framework, in which calculation of interesting properties of the system lies within the range of numerical and analytical methods.

In this chapter, we present two classical field theories for interacting bosons. We start with a short review of a well-known GP equation [14]. We derive it, paying attention to the range of applicability of the approximation. In the next step, we present a theory build on the hydrodynamic approach that aims to describe Bose gas with an arbitrarily strong interactions. We discuss differences with GP equation and present benchmarks with exact solutions from the LL model.

2.1. Gross-Pitaevskii equation

The most widely used approach to study cold Bose gases is the mean-field approximation. The range of validity of this method is restricted to weak interparticle interactions and to low-energy regime (namely, close to the ground state). It heavily relies on the observation, that in the case of an ideal Bose gas at $T = 0$, all the atoms occupy the same single-particle

quantum state. Therefore, the many-body wave function is a product

$$\Psi_{\mathrm{GS}}^{\mathrm{ideal}}(x_1,\ldots,x_N)=\prod_{j=1}^{N}\phi_{\mathrm{GS}}(x_j). \tag{2.2}$$

Let us now depart from the trivial example of ideal gas and move to the regime of weak interparticle interactions. The mean-field approximation assumes that the factual ground state remains in the product form. The effect of interactions is visible only in the modified form of the single particle orbital $\phi_{\mathrm{GS}}(x)\to\phi(x)$. However, at this point we do not know the specific form of $\phi(x)$, which is determined it in the following way. We calculate the expectation value of the Hamiltonian (2.1) on the product state build with an unknown function $\phi(x)$. Such a quantity may be interpreted as an energy functional of a field $\phi(x)$

$$E[\phi]:=-N\frac{\hbar^2}{2m}\int dx\phi^*(x)\partial_x^2\phi(x)+\frac{N(N-1)}{2}\int dxdx'\phi^*(x)\phi^*(x')V(x-x'))\phi(x')\phi(x). \tag{2.3}$$

We demand that the optimal orbital $\phi(x)$ minimizes the functional (2.3). This is equivalent to the standard extremal condition $\frac{\delta E}{\delta\phi^*}=0$ supplemented with the normalization constraint $\int dx|\phi(x)|^2=1$. Such a constraint is properly taken into account by an introduction of a Lagrange multiplier μ. Explicitly, minimization condition reads

$$\mu\phi(x)=-\frac{\hbar^2}{2m}\partial_x^2\phi(x)+(N-1)\int dx'V(x-x')|\phi(x')|^2\phi(x). \tag{2.4}$$

The is the stationary GP equation, which is routinely solved for different interaction potentials $V(x-x')$ using so-called imaginary time evolution (ITE) method (see Appendix A for details). The solution also gives μ which is referred to as the chemical potential.

Complementary to the stationary equation, we may consider a dynamical situation, where the orbital $\phi(x,t)$ depends on time t. We still assume the many body wave function remains to be a product state during the evolution, limiting ourselves to low-energy dynamics. The time-dependent version of GP equation reads

$$i\hbar\partial_t\phi(x,t)=-\frac{\hbar^2}{2m}\partial_x^2\phi(x,t)+(N-1)\int dx'V(x-x')|\phi(x',t)|^2\phi(x,t). \tag{2.5}$$

GP equation proved to be an extremely successful approach to weakly interacting bosons, not only in 1D, but also in two- and three-dimensional systems. It provides correct description of a variety of phenomena such as solitons or low-energy excitations [15].

However, in this thesis we want to deal with strongly interacting systems, for which product ansatz must fail, as it neglects interparticle correlations that are inevitable for strong repulsion. At the same time, we aim for a relatively simple theory that captures at least some of the relevant properties of the system. Such a theory is derived in the remaining part of the present chapter.

2.2. Hydrodynamic theory for the Bose gas with arbitrarily strong interactions

At this point we specify the form of interparticle potential to be $V(x-x')=g\delta(x-x')$, $g>0$. As indicated earlier, such a system with contact interactions is exactly solvable and the solutions were provided by Lieb and Liniger in 1963 [12, 13]. In the thermodynamic limit

given by the conditions $N/L = \text{const}$, $N, L \to \infty$ the energy of the ground state may be written as [13]

$$E_0[N, L] = \frac{\hbar^2}{2m}\frac{N^3}{L^2}e_{\mathrm{LL}}(\gamma) \tag{2.6}$$

with the important parameter $\gamma = \frac{m}{\hbar^2}\frac{gL}{N}$. The function $e_{\mathrm{LL}}(\gamma)$ is given by a system of integral equations, however it can be accurately approximated by known and simple functions of γ (see Appendix B). For weak interactions, when $\gamma \ll 1$, we have $e_{\mathrm{LL}}(\gamma) \approx \gamma$, whereas for $\gamma \to \infty$ we recover the ground state energy of the Tonks-Girardeau gas [16] of infinitely repulsive bosons with $e_{\mathrm{LL}}(\gamma) \to \frac{\pi^2}{3}$. With the equation of state (2.6) at hand, we may calculate the pressure and the chemical potential in the following way

$$P_{\mathrm{LL}}[N/L] = -\frac{\partial E_0[N, L]}{\partial L} = \frac{\hbar^2}{2m}\frac{N^3}{L^3}\left(2e_{\mathrm{LL}}(\gamma) - \gamma e'_{\mathrm{LL}}(\gamma)\right), \tag{2.7a}$$

$$\mu_{\mathrm{LL}}[N/L] = \frac{\partial E_0[N, L]}{\partial N} = \frac{\hbar^2}{2m}\frac{N^2}{L^2}\Big(3e_{\mathrm{LL}}(\gamma) - \gamma e'_{\mathrm{LL}}(\gamma)\Big). \tag{2.7b}$$

The energy given by formula (2.6) is a result of an exact calculation, therefore even in the strong repulsion limit it properly accounts for interparticle correlations. The same is true for the pressure and the chemical potential. The precious informations contained in the function $e_{\mathrm{LL}}(\gamma)$ will be a crucial building block used to construct a hydrodynamic theory of a gas with interactions of arbitrary strength. In the following derivation, we take another approach and refer to hydrodynamic equations, in contrast to the GP equation.

Instead of using a wave function, we aim to characterize our gas with two classical fields $\rho(x)$ and $v(x)$ as in the classical theory of continous media. The first one corresponds to the local density of the atomic cloud, whereas the other is the velocity of a collective motion of the particles. The continuity equation reads

$$\partial_t \rho + \partial_x(\rho v) = 0, \tag{2.8}$$

while the Euler equation has the following form

$$\partial_t v + v\partial_x v = \frac{1}{m\rho}\partial_x P, \tag{2.9}$$

where P is the pressure at the position x. It is worthwhile to recall some basic assumptions of the hydrodynamics. The system is divided into small parts of length dx, which are much smaller than the system size L but at the same time are much larger than the interparticle distances. Moreover, local equilibrium hypothesis assumes that equilibrium thermodynamics holds for individual parts with size dx. Having that scale hierarchy in mind, we approximate the energy of an element with energy density given by (2.6). Moreover, from the local equilibrium hypothesis we assume that the pressure inside the element is given by the formula (2.7a). Using the identity $\frac{1}{\rho}\partial_x P_{\mathrm{LL}} = -\partial_x \mu_{\mathrm{LL}}$ we bring the Euler equation to the form

$$\partial_t v + v\partial_x v = -\frac{1}{m}\partial_x \mu_{\mathrm{LL}}. \tag{2.10}$$

Next, we replace the two real fields $v(x)$ and $\rho(x)$ with a single complex field

$$\phi(x) = \sqrt{\rho/N}e^{i\varphi} \tag{2.11}$$

with $\hbar\,\partial_x\varphi = mv$. Then, the hydrodynamical equations discussed above may be combined into

$$i\hbar\frac{\partial}{\partial t}\phi = -\frac{\hbar^2}{2m}\frac{\partial^2\phi}{\partial x^2} + \mu_{\mathrm{LL}}\left[N|\phi|^2\right]\,\phi, \tag{2.12}$$

with

$$\mu_{\mathrm{LL}}\left[N|\phi|^2\right] = \frac{\hbar^2}{2m}N^2|\phi|^4\left(3e_{\mathrm{LL}}\left(\frac{\kappa}{N|\phi|^2}\right) - \frac{\kappa}{N|\phi|^2}e'_{\mathrm{LL}}\left(\frac{\kappa}{N|\phi|^2}\right)\right) \tag{2.13}$$

where $\kappa := \frac{gm}{\hbar^2}$. The equation (2.12) is called the Lieb-Liniger Gross-Pitaevskii (LLGP) equation and will be our main tool to deal with strongly repulsive bosons on the mean-field level. It is important to note, that we neglected so-called quantum pressure term as we went from the hydrodynamical equations to (2.12). It was pointed out in [17], that this is justified as long as we consider slowly-varying density profiles. In this thesis, we focus on long-wavelength excitations fulfilling that assumption.

Let us emphasize that the LLGP equation was studied before in various contexts and appeared under different names [18, 19]. The $g \to \infty$ limit version was introduced by Kolomeisky [20] and was later criticized by Girardeau and Wright [21] for incorrect description of dynamics involving rapidly-varying density profiles. On the other hand, the full equation involving function $e_{\mathrm{LL}}(\gamma)$ was used for the descrpition of shock waves [17].

One should interpret $\phi(x)$ cautiously. From our construction we see, that *a priori* it has nothing to do with a wave function. On the other hand, equation (2.12) resembles GP equation. Indeed, for contact interactions GP equation takes the form

$$i\hbar\partial_t\phi(x,t) = -\frac{\hbar^2}{2m}\partial_x^2\phi(x,t) + g(N-1)|\phi(x,t)|^2\phi(x,t). \tag{2.14}$$

If we consider limit of small interactions, then the function $e_{\mathrm{LL}}(\gamma)$ may be approximated by $e_{\mathrm{LL}}(\gamma) \approx \gamma$. Applying this approximation to (2.12), together with the condition of large particle number $N \approx N-1$ we recover the GP equation. It means that for a weakly interacting gas, we actually can interpret $\phi(x)$ as a wave function, having in mind the derivation of GP equation. Importantly, this is certainly not the case in the regime of strong repulsion, where $\phi(x)$ should be interpreted as an auxiliary field, conveniently representing hydrodynamic quantities parametrizing our system.

For further analysis it is useful to note that the equation (2.12) may be derived in a different way, namely using a variational treatment of the energy functional

$$E_{\mathrm{LLGP}}[\phi] = \frac{N\hbar^2}{2m}\int dx\Big[\left|\frac{d\phi}{dx}\right|^2 + N^2|\phi|^6 e_{\mathrm{LL}}\left(\frac{\kappa}{N|\phi|^2}\right)\Big]. \tag{2.15}$$

It is quite natural to ask what is the purpose for constructing an effective description of integrable model, for which almost everything is known. Contrary to the Bethe Ansatz techniques that provide a solution to the Lieb-Liniger model, hydrodynamic approach is also capable of describing gas in confined geometries and in the case of non-contact interactions. In the next chapter, we will extend interactions in our model by adding attractive, dipolar part.

Let us remind that the ultimate goal of this work is to describe the low-energy excitations of quantum droplets described with the LLGP equation further extended by the dipolar interactions. In order to understand if our approach is capable of doing that, we study elementary excitations displayed by purely repulsive gas calculated from our approach and compare to exact results from the LL model. This will give us some intuition whether the seemingly crude hydrodynamic approximation can be used to correctly describe low-energy modes of quantum droplets characterized by strong interparticle interactions.

2.2.1. Elementary excitations

We wish to study response of a homogenous gas with $\phi_0(x) = \frac{1}{\sqrt{L}}$ to some small initial perturbation. We will characterize the response by identifying collective modes and excitation

energies. Collective modes are understood in the same way as the modes in classical model systems such as chains of oscillators. When the system is driven out of equilibrium in a way given by the shape of the mode, it oscillates forever with the frequency given by the excitation energy. Moreover, the evolution of any small initial perturbation may be obtained by the decomposition in the basis of collective modes for which the time evolution is known and given by the oscillatory motion with respective frequency. In order to find the collective modes, we consider a standard ansatz for the time-dependent field $\phi(x,t)$, namely [15]

$$\phi(x,t) = \Big(\phi_0(x) + \delta\phi(x,t)\Big)e^{-i\mu_{\mathrm{LL}}[N/L]t/\hbar}, \tag{2.16}$$

where

$$\delta\phi(x,t) = u(x)e^{-i\epsilon t/\hbar} + v^*(x)e^{i\epsilon t/\hbar} \tag{2.17}$$

is assumed to be a small deviation from the uniform state. We change the notation used in the discussion of hydrodynamic equations and from now $v(x)$ no longer denotes velocity field of the gas. We see that the functions $u(x)$ and $v(x)$ determine the spatial dependence of the density deviation, whereas ϵ sets its characteristic time scale. In order to determine the allowed shapes of excitations (collective modes) $u(x), v(x)$ and the corresponding excitation energies ϵ we plug ansatz (2.16) into the equation of motion (2.12), keeping terms at most linear at $\delta\phi$. Using the fact, that $\phi_0(x)$ is a stationary solution with corresponding chemical potential $\mu = \mu_{\mathrm{LL}}[N/L]$, we get

$$i\hbar\partial_t\delta\phi = \Big[-\frac{\hbar^2}{2m}\partial_x^2 + mv_{\mathrm{LL}}^2[N/L]\Big]\delta\phi + mv_{\mathrm{LL}}^2[N/L]\delta\phi^*, \tag{2.18}$$

where $v_{\mathrm{LL}}[N/L] = \frac{\hbar N}{mL}\sqrt{3e_{\mathrm{LL}}(\gamma) - 2\gamma e'_{\mathrm{LL}}(\gamma) + \frac{1}{2}\gamma^2 e''_{\mathrm{LL}}(\gamma)}$ is an exact expression for the speed of sound in LL model [12, 22]. Plugging our ansatz for $\delta\phi$, see (2.17), we arrive at

$$\epsilon u(x) = \Big(-\frac{\hbar^2}{2m}\partial_x^2 + mv_{\mathrm{LL}}^2[N/L]\Big)u(x) + mv_{\mathrm{LL}}^2[N/L]v(x), \tag{2.19a}$$

$$-\epsilon v(x) = \Big(-\frac{\hbar^2}{2m}\partial_x^2 + mv_{\mathrm{LL}}^2[N/L]\Big)v(x) + mv_{\mathrm{LL}}^2[N/L]u(x). \tag{2.19b}$$

From the translational invariance of the system, it follows that we can consider u and v as $u(x) = ue^{ipx/\hbar}$ and $v(x) = ve^{ipx/\hbar}$ with $p = 0, \pm\frac{2\pi\hbar}{L}, \pm\frac{4\pi\hbar}{L}, \ldots$, which gives

$$\epsilon u = \frac{p^2}{2m}u + (u+v)mv_{\mathrm{LL}}^2[N/L], \tag{2.20a}$$

$$-\epsilon v = \frac{p^2}{2m}v + (u+v)mv_{\mathrm{LL}}^2[N/L]. \tag{2.20b}$$

We solve these equations obtaining the excitation spectrum

$$\epsilon(p) = \sqrt{(v_{\mathrm{LL}}[N/L]p)^2 + \Big(\frac{p^2}{2m}\Big)^2}. \tag{2.21}$$

We omit the analysis of the density perturbation profiles $u(x)$ and $v(x)$. The purpose of this section is to compare excitation energies. The analysis of the shapes of collective modes will be performed in details in the case of quantum droplets. The result (2.21) may be directly compared with the excitation spectrum found in the exact many-body treatment of LL model. However, we must be careful at this point because LL model exhibits two different branches of

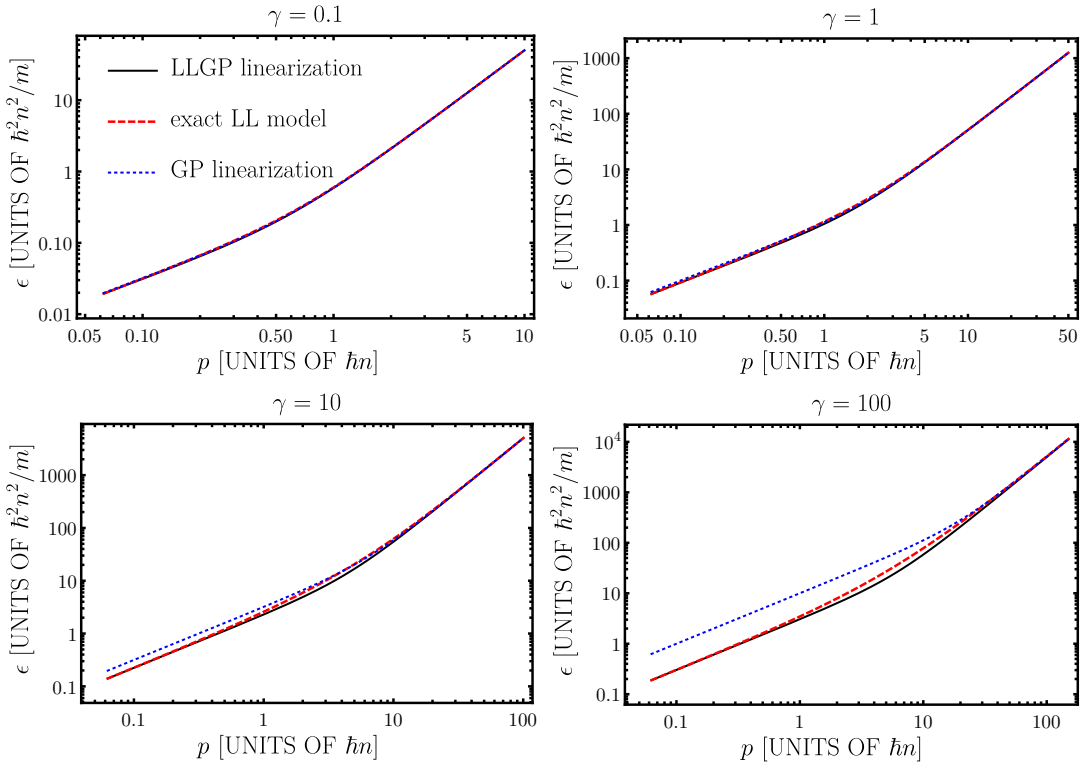

Figure 2.1: Energies of elementary excitations ϵ as a function of momentum p for different interaction strenghts γ. We compare energies found in effective approaches (GP and LLGP) and exact results for the LL model. Results from the LLGP agree with the predictions of LL model in the regimes of small and large momenta, contary to the GP equation that predicts incorrect speed of sound governing low-momentum asymptotics of ϵ for sufficiently strong interactions γ.

elementary excitations $\epsilon_I(p)$ and $\epsilon_{II}(p)$ [13], called phononic and solitonic branch, respectively. Importantly, for the first branch, in the limit of small momenta p one recovers linear dispersion relation

$$\epsilon_I(p) \overset{p\to 0}{\approx} v_{\mathrm{LL}}[N/L]|p|, \tag{2.22}$$

at the same time, for large momenta we get quadratic dispersion of a free particle

$$\epsilon_I(p) \overset{p\to\infty}{\approx} \frac{p^2}{2m}. \tag{2.23}$$

It turns out that the result (2.21) coincides with either (2.22) or (2.23) for very small or very large p, correspondingly. Importantly, the agreement holds for any interaction strength.

This a promising result regarding the low-energy excitations of quantum droplets, because by comparing our approach with the LL model we see, that hydrodynamic description may correctly capture energies of excitations also in the strongly interacting regime, far beyond the regime of weak interparticle correlations.

Lastly, let us note that a similar procedure may be carried out for the GP equation. In this case, one recovers the same expression for the excitation energy as in (2.21) but with a different speed of sound $v_{\mathrm{GP}}[N/L] := \sqrt{gN/mL}$. Values of v_{GP} and v_{LL} coincide for small interaction strength γ, but not surprisingly $v_{\mathrm{GP}}[N/L]$ fails completely when γ is large as it predicts a diverging speed of sound in contrast to $v_{\mathrm{LL}}[N/L] \overset{\gamma\to\infty}{\to} \frac{\pi\hbar N}{mL}$. Once again, this

observation supports the claim that the GP equation cannot be used to describe strongly interacting bosons.

Summing up, we have presented a hydrodynamic approach that correctly describes low-energy excitations of strongly repulsive gas. In the next chapter, we will extend it by including attractive dipolar interactions.

Chapter 3

Phases of strongly interacting dipolar gas

In this chapter we describe atoms with magnetic moments μ_D polarized along X axis, trapped in a tight harmonic trap in Y and Z directions, but free to move in the X direction.

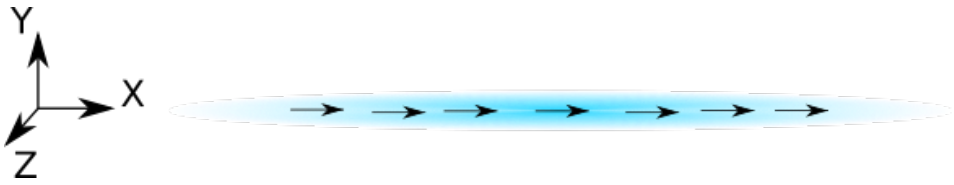

Figure 3.1: Sketch of the system under study: polarized dipolar gas in one dimension.

In general, the total interaction potential between atoms in such setup reads

$$V(x-x') = g\delta(x-x') - g_{\mathrm{dd}} V^{\sigma}_{\mathrm{dd}}(x-x'), \tag{3.1}$$

with the long-range part of effective quasi-1D dipolar potential [23] given by

$$V^{\sigma}_{\mathrm{dd}}(x-x') = \frac{v(\frac{x-x'}{\sigma})}{\sigma}, \quad v(u) = \frac{1}{4}\left(-2|u| + \sqrt{2\pi}(1+u^2)e^{u^2/2}\mathrm{Erfc}(|u|/\sqrt{2})\right) \tag{3.2}$$

and

$$g_{\mathrm{dd}} = -\frac{\mu_0 \mu_D^2}{4\pi}\frac{1-3\cos^2\theta}{\sigma^2}. \tag{3.3}$$

Here, $\sigma = \sqrt{\frac{\hbar}{m\omega_\perp}}$ denotes oscillator length of transversal harmonic confinement with frequency $\omega_\perp$. The character of the interaction strongly depends on the angle θ defined in Fig. 3.2. We

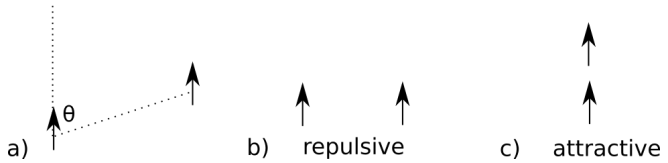

Figure 3.2: Panel a): Character of the dipolar interaction strongly depends on the angle θ. In b) we see configuration for which interactions are repulsive. We are interested in head-to-tail configuration presented in c), for which interactions are attractive.

focus on the attractive dipolar interactions, corresponding to configuration with angle $\theta = 0°$ and $g_{\rm dd} > 0$. As illustrated in Fig. 3.3 the length scale σ is directly related to the range of the potential. When $\sigma \to 0$, $V^{\sigma}_{\rm dd}(x)$ acquires a form of a delta peak [23] $V^{\sigma}_{\rm dd}(x) \to \delta(x)$. For large arguments, the potential is characterized by the standard dipolar decay $V^{\sigma}_{\rm dd}(x) \sim \frac{1}{x^3}$ [23].

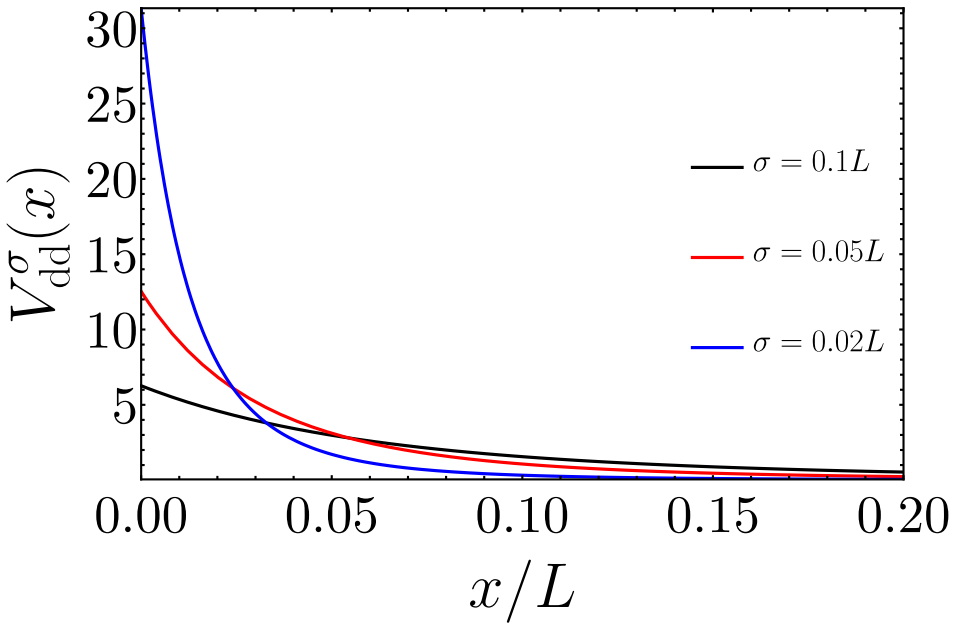

Figure 3.3: Dipolar interaction potential for different confinement length scales σ related to the range of the potential.

Finally, let us note that the dipolar potential $V^{\sigma}_{\rm dd}(x-x')$ integrates to unity [23], therefore the parameter $g_{\rm dd}$ directly measures the strength of the dipolar attraction.

3.1. LLGP with dipolar interactions

In order to include dipolar forces in our model we work with the variational framework used in the derivation of the LLGP equation. We need to generalize the energy functional (2.15) by adding the energy related to dipolar interparticle interactions. Let us note that in the full many-body picture, expectation value of the dipolar interaction energy calculated on a given state may be written as

$$\langle \hat{V}_{\rm dd} \rangle = \int dxdy\, G_2(x,y) V^{\sigma}_{\rm dd}(x-y) \tag{3.4}$$

where $G_2(x,y) = \langle \hat{\Psi}^{\dagger}(x)\hat{\Psi}^{\dagger}(y)\hat{\Psi}(y)\hat{\Psi}(x)\rangle$ denotes the second order correlation function and $\hat{\Psi}(x)$ is the bosonic field operator. Obviously, we do not know the explicit form of the $G_2(x,y)$. However, one can anticipate some features of it having in mind the context of quantum droplets with strong, contact interactions close to the fermionization regime. This characteristic features discussed below will allow us to approximate (3.4) with a functional of the field $\phi(x)$.

Firstly, we discuss the second order correlation function in the TG regime of infinitely repulsive bosons, $G^{\rm TG}_2(x,y)$, where it may be explicitly calculated for the ground state. The translational invariance implies that the function depends only on the distance between particles, therefore we define $G^{\rm TG}_2(x-y) := G^{\rm TG}_2(x,y)$, shown in Fig. 3.4. Due to the inifitely

strong repulsion G_2^{TG} vanishes at the diagonal $x = y$. For distances much longer than the interparticle distance $d := L/N$, i.e. $|x - y| \gg d$, the correlation function tends to 1.

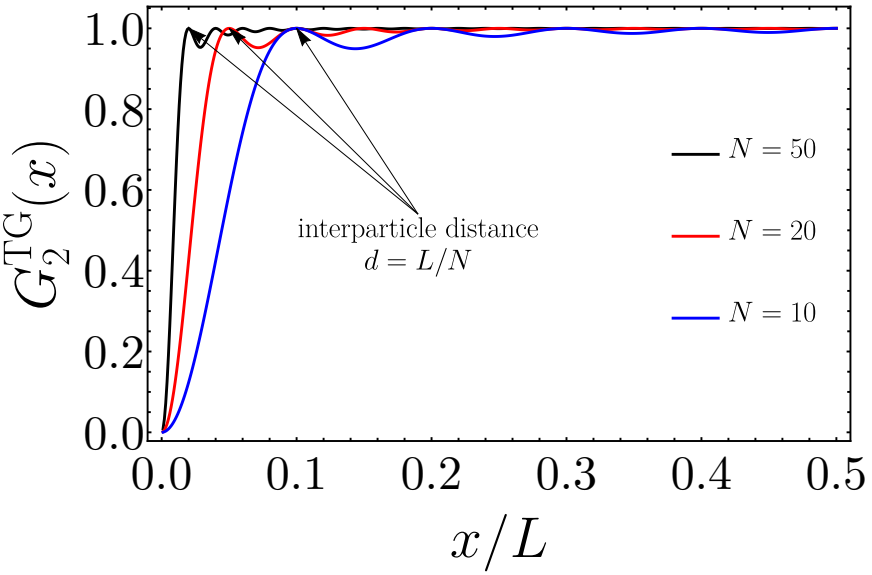

Figure 3.4: Second order correlation function calculated for the ground state of TG gas. Due to fermionization, $G_2^{\mathrm{TG}}(0) = 0$ and the first maximum is reached around the point corresponding to interparticle distance $x = d$. We see that d sets up the characteristic length scale for the function i.e. for $x \gg d$, $G_2^{\mathrm{TG}}(x) = 1$.

Let us now discuss the possible impact of attractive dipolar interactions on the G_2 function. In such cases one expects bound states, for which the translational symmetry is broken. The function $G_2(x, y)$, known as the density-density correlation, is small at these positions x and y where the density of the gas is very low. To account for this fact, one may approximate the second order correlation function by $G_2(x, y) = \rho(x)\rho(y)$, where $\rho(x)$ is the gas density. This formula works excellently for the weak, purely attractive contact interaction, when atoms form a bright solitons and the density is evaluated with the GP equation.

Combining these two observations, we propose the following form of the second order correlation

$$G_2(x, y) = G_2^{\mathrm{TG}}(x - y)\rho(x)\rho(y). \tag{3.5}$$

Such a form takes into account both, the fermionization ($G_2(x, y) = 0$ for $x = y$) and the impact of the gas inhomogenity. We assume the correlation function in the form (3.5) and simplify the expression for the dipolar energy (3.4). Throughout this work, we will work in the regime of long-range dipolar interactions with $\sigma \gg d$. Hence, under the integral (3.4) we may treat the function $G_2^{\mathrm{TG}}(x - y)$ as constant as it differs from 1 only at the very small part of the integration domain, i.e. in a narrow stripe of width d around the line $x = y$. After this approximation, the functional for the total energy reads

$$\begin{aligned} E[\phi] = N \int dx \Big[\frac{\hbar^2}{2m} \left| \frac{d\phi}{dx} \right|^2 + \frac{N^2\hbar^2}{2m} |\phi|^6 e_{\mathrm{LL}} \left(\frac{\kappa}{N|\phi|^2} \right) + \\ - \frac{1}{2} N g_{\mathrm{dd}} \int dx' V_{\mathrm{DD}}^{\sigma}(x - x') |\phi(x)|^2 |\phi(x')|^2 \Big]. \end{aligned} \tag{3.6}$$

Finally, applying the least action principle we obtain the extended LLGP equation

$$i\frac{\partial}{\partial t}\phi = -\frac{1}{2}\frac{\partial^2\phi}{\partial x^2} + \mu_{\mathrm{LL}}\left[N|\phi|^2\right]\,\phi - g_{\mathrm{dd}}N\int dx' V_{\mathrm{dd}}^{\sigma}(x-x')|\phi(x')|^2\phi(x), \tag{3.7}$$

where we use $\hbar = m = 1$ in consistency with [11]. An alternative justification of the LLGP equation may be found in the Supplemental Materials of [11]. Additionally, a comparison between effective equation (3.7) and results stemming from the full diagonalization of many-body Hamiltonian for small systems can also be found in the same paper.

Note, that although we focused on the regime of strong contact repulsion $\gamma \gg 1$, and long-range dipolar interactions $\sigma \gg d$, we are still left with an equation involving four parameters: N, g, g_{dd} and σ. In the next section, we study the solution to the equation (3.7) to characterize different parameter regimes.

3.2. Stationary solutions in different regimes

Having the full equation (3.7) derived we may play with the parameters and observe, how changes of respective parameters influence the resulting stationary solution. We divide the stationary solutions into three classes: uniform solution, quantum droplet and bright soliton. Description of these families of solutions is done in the remaining part of this section.

3.2.1. Uniform solution

In the previous chapter we focused on the case of purely repulsive gas. In such case, stationary solution corresponds to the uniform gas density $\phi_{\mathrm{GS}}(x) = 1/\sqrt{L}$. Additional weak attractive dipolar interaction does not change this phase and we may readily write down the expression for the chemical potential

$$\mu = \mu_{\mathrm{LL}}[N/L] - g_{\mathrm{dd}}\frac{N}{L}. \tag{3.8}$$

However, for sufficiently large g_{dd} the ground state becomes a bound state, i.e. a quantum droplet or a soliton. This is a phase transition accompanied by the translational symmetry breaking.

3.2.2. Quantum droplets

The first discussed phase with broken translational symmetry is the quantum droplet. Here, we start by paying a special attention to the limit $g \to \infty$ that significantly simplifies analysis of the LLGP equation.

Fermionized quantum droplets

In the regime $g \to \infty$ the LL energy reads $e_{\mathrm{LL}}(\gamma \to \infty) = \frac{\pi^2}{3}$ and the stationary LLGP equation takes the form

$$\mu\phi = -\frac{1}{2}\frac{\partial^2\phi}{\partial x^2} + \frac{\pi^2 N^2}{2}|\phi|^4\phi - g_{\mathrm{dd}}N\int dx' V_{\mathrm{dd}}^{\sigma}(x-x')|\phi(x')|^2\phi(x). \tag{3.9}$$

As shown in Fig. 3.5, sufficiently strong attraction breaks the translational invariance and the stationary solution takes the form of a quantum droplet. In the specific case of $N = 500$ considered here this happens between $g_{\mathrm{dd}} = 100$ and $g_{\mathrm{dd}} = 140$.

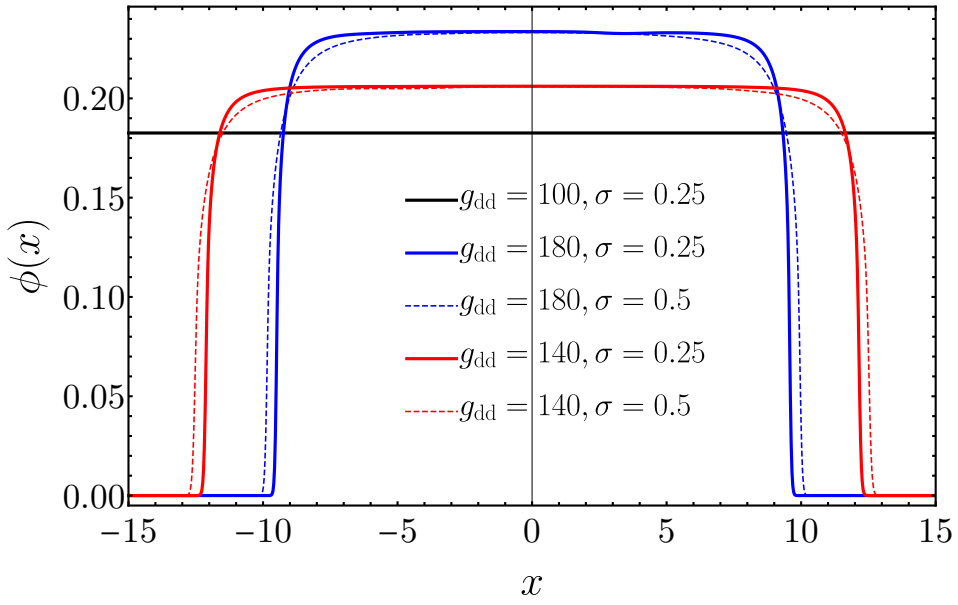

Figure 3.5: Stationary solutions to the (3.9) for $N = 500$ and different interaction parameters.

One observes in Fig. 3.5, that the density profile of a droplet is characterized by a flat top region with an approximately constant density and the edges, where the density rapidly drops. Not surprisingly, the droplet becomes narrower as we increase dipolar attraction $g_{\rm dd}$. Note that the range of dipolar interactions σ affects mainly the edges and does not influence the bulk density of the droplet (compare dashed and solid lines).

Fermionized quantum droplets - analytical regime

We observe in the numerical simulations, that when the number of atoms increases, the droplet becomes wider, whereas the width of the edge remains practically constant. Therefore one may expect that the edge profile becomes irrelevant for some observables in the limit of large particle number. In the previous section we have observed that the interaction range σ influences mainly the edges. Thus, in the regime of wide droplets majority of the observables should not be sensitive to the interaction range, as long as σ is much smaller than the width of the droplet W. In particular, taking the limit $\sigma \to 0$ should not change the profile significantly in comparison to the profile obtained for some finite value $\sigma \ll W$. In such a limit, the dipolar potential tends to delta function and the equation (3.9) acquires the following form

$$\mu\phi = -\frac{1}{2}\frac{\partial^2\phi}{\partial x^2} + \frac{\pi^2 N^2}{2}|\phi|^4\phi - g_{\rm dd}N|\phi|^2\phi. \tag{3.10}$$

One can derive the analytical form of the ground state of the latter equation [24]

$$\phi(x) = \sqrt{\frac{3\beta}{4\alpha}}\frac{\tanh\eta}{\sqrt{1+\operatorname{sech}\eta\cosh(x/a)}}, \tag{3.11}$$

where we introduced the following coefficients

$$\alpha = \frac{\pi^2 N^2}{2} \qquad \beta = g_{\rm dd}N \qquad \eta = \sqrt{\frac{2\alpha}{3}} \qquad a = \frac{1}{\beta}\frac{\eta}{\tanh\eta}. \tag{3.12}$$

The chemical potential is calculated as follows

$$\mu = \int dx \Big(\frac{1}{2} |\partial_x \phi|^2 + \frac{\pi^2 N^2}{2} |\phi|^6 - g_{\mathrm{dd}} N |\phi|^4 \Big). \tag{3.13}$$

Exemplary solutions are presented in Fig. 3.6. As expected, droplets become wider with the growing number of particles.

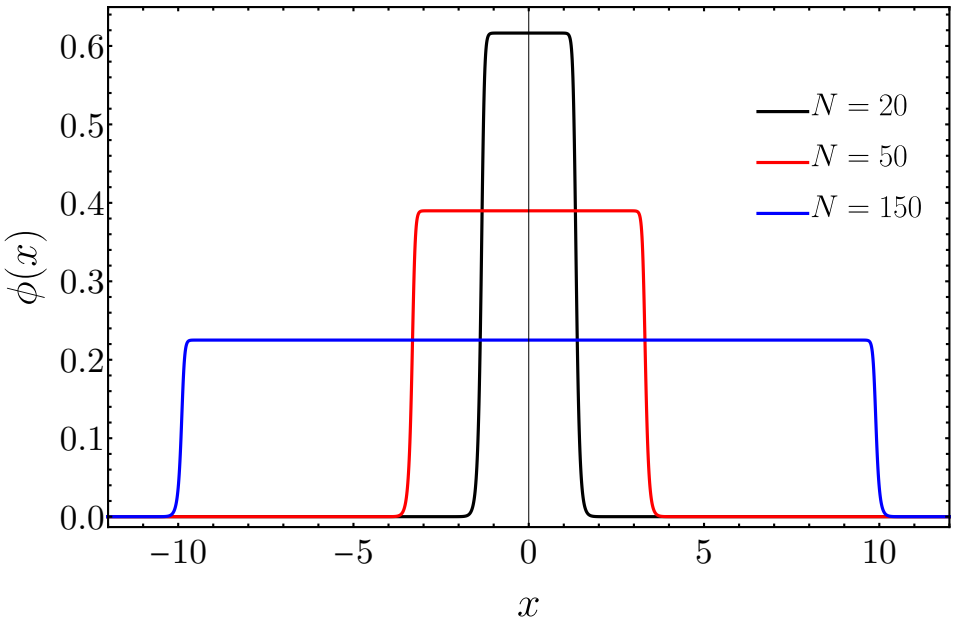

Figure 3.6: Density profiles given in Eq. (3.10) for $g_{\mathrm{dd}} = 50$ and different particle numbers.

For large N, the density profile (3.11) tends to a rectangular shape with the height

$$\rho_0 = \frac{3\beta}{4\alpha} = \frac{3 g_{\mathrm{dd}}}{2\pi^2 N} \tag{3.14}$$

and with the width $W = \rho_0^{-1} = \frac{2\pi^2 N}{3 g_{\mathrm{dd}}}$.

One may question the validity of the limit $\sigma \to 0$ taken in (3.10), as our derivation of the LLGP equation assumed that the range of interactions is much larger than the inter-particle distance, i.e. $d \ll \sigma$. Although we explicitly considered the limit $\sigma \to 0$, the large droplet limit assumes only $\sigma \ll W$. Equation (3.10) should be valid in the regime, where both conditions are fulfilled, i.e. when we have the following scale hierarchy $d \ll \sigma \ll W$. Such a regime is investigated in Fig. 3.7. In this regime we observe that solutions of equations (3.10) and (3.9) almost overlap. The widths and bulk densities agree, the only difference is visible in a small region near the edges of the droplets. What is more, we see clearly that the exact solution (3.11) approaches a rectangular profile. Later on, we will use such profile as an Ansatz to derive analytically properties of the low-energy excitations in the considered regime.

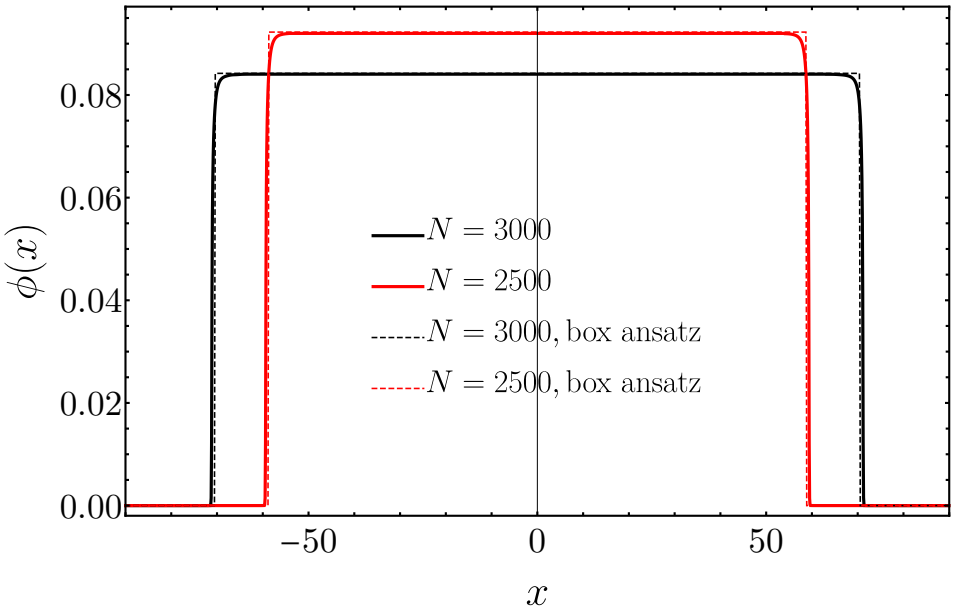

Figure 3.7: Stationary solutions to the Eq. (3.10) (solid lines) versus solutions to the non-local Eq. (3.9) (dashed lines) for finite $\sigma = 0.25$. The dipolar attraction equals $g_{\rm dd} = 140$ and the inter-particle distance $d \approx 0.047$. The solutions to the Eq. (3.9) is indistinguishable from the box ansatz prediction.

Quantum droplets for finite repulsion

Here, we present a short analysis of a generic stationary solutions for a finite repulsion g. We will consider a specific case of $g = 250, g_{\rm dd} = 180, N = 200, \sigma = 0.05$ and observe, how te change of parameters $g, g_{\rm dd}, N, \sigma$ affects the stationary solution.

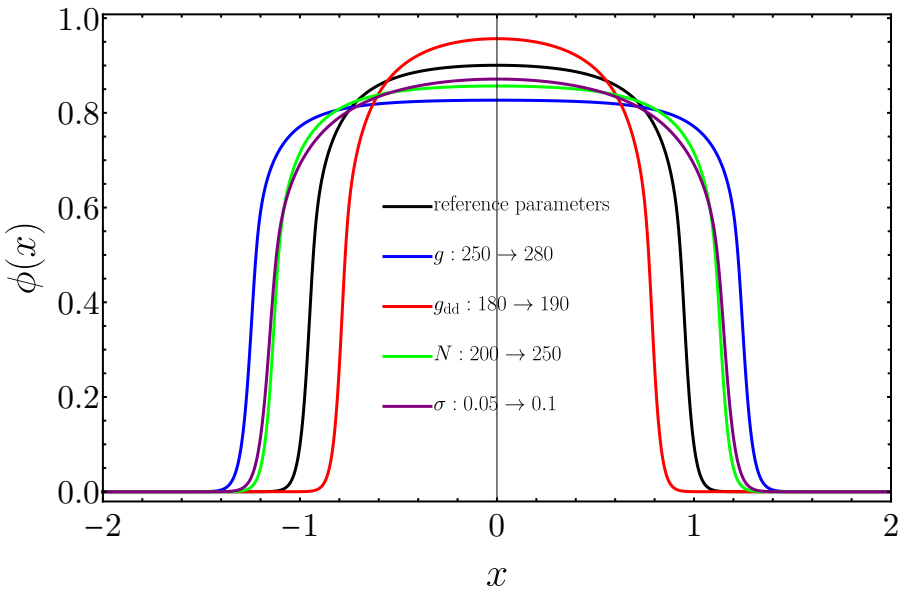

Figure 3.8: Stationary solutions to the (2.12) for different parameters. We consider a reference solution obtained for $g = 250, g_{\rm dd} = 180, N = 200, \sigma = 0.05$ and study how the change of the parameters affects the stationary solution.

From the Fig. 3.8 we may draw the following observations:

- Increasing the contact repulsion g results in a wider droplet.
- Increasing the dipolar attraction g_{dd} results in a narrower droplet.
- Increasing the particle number N results in a wider droplet.
- Increasing the interaction range σ rounds the flat-top part (note that we previously noted that for $\sigma \to 0$ we get almost perfect flat top well approximated by rectangular shape).

Rectangular ansatz for quantum droplets

To complete the discussion we propose some analytical understanding of quantum droplets in our model. Given the above observations of the flat-top shape of a droplet, one can come up with an approximate ansatz in a form of a rectangular solution

$$\phi(x) = \frac{1}{\sqrt{W}}\mathrm{rect}(x/W), \tag{3.15}$$

where the width W is the only parameter of the ansatz. In the following considerations we also neglect the kinetic energy. In the range of checked parameters it is justified, as the kinetic energy is dominated by the energy stemming from interactions.

We plug the rectangular ansatz into the energy functional [Eq.(3.6) with neglected kinetic energy term] and calculate its derivative with respect to W looking for a minimum

$$\frac{dE}{dW} = \frac{1}{2}N^3\left[-\frac{2}{W^3}e_{\mathrm{LL}}\Big(\frac{gW}{N}\Big) + \frac{1}{W^3}\frac{gW}{N}e'_{\mathrm{LL}}\Big(\frac{gW}{N}\Big)\right] + g_{\mathrm{dd}}\frac{N^2}{2W^2} = 0. \tag{3.16}$$

The equation above may be cast in a compact equation

$$\frac{1}{\gamma_W}\big(2e_{\mathrm{LL}}(\gamma_W) - \gamma_W e'_{\mathrm{LL}}(\gamma_W)\big) = g_{\mathrm{dd}}/g, \tag{3.17}$$

with W hidden in $\gamma_W := gW/N$. Additionally, one may calculate the corresponding chemical potential in the rectangular approximation

$$\mu = \mu_{\mathrm{LL}}[N/W] - g_{\mathrm{dd}}\frac{N}{W}. \tag{3.18}$$

In the next chapters we will extensively use the rectangular ansatz and formulae for W and μ to derive analytically the energies and spatial dependence of elementary excitations in a quantum droplet.

3.2.3. Bright solitons

Bright solitons are the last phase found in our model. They may appear when the finite contact repulsion is less significant than the attractive dipolar forces.

On the level of the density profiles we see that for sufficiently large g_{dd}, the flat-top profile is replaced with a well-defined maximum of soliton-like shape.

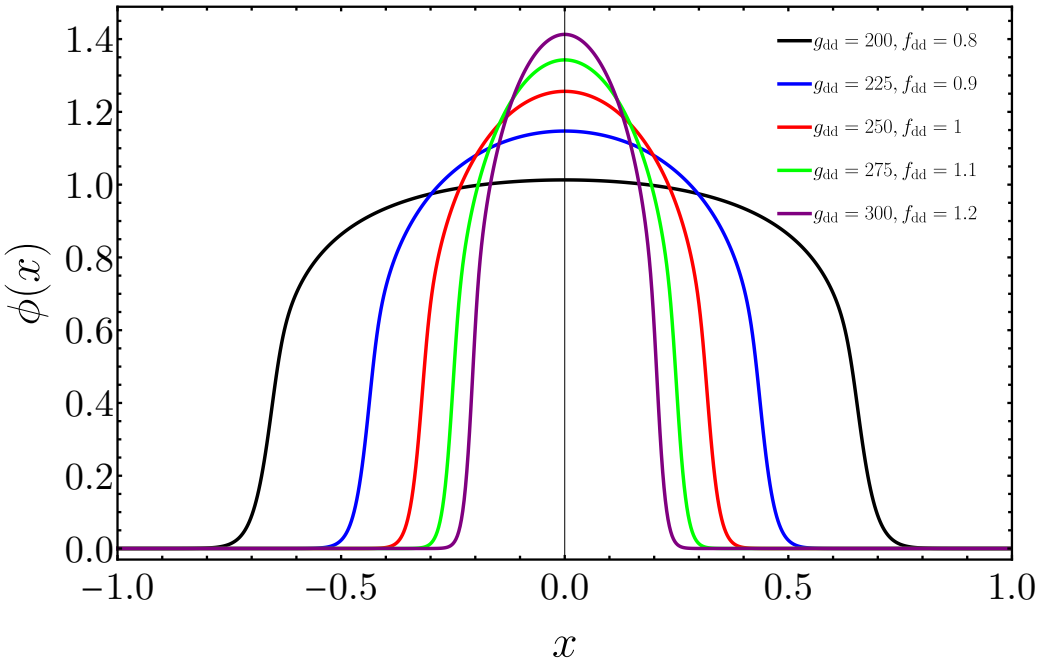

Figure 3.9: Droplet-soliton transition driven by changing g_{dd} for $g = 250$, $N = 200$ and $\sigma = 0.05$.

It is suggested in Ref. [11] that some form of a transition occurs around $f_{\mathrm{dd}} = g_{\mathrm{dd}}/g = 1$. For $f_{\mathrm{dd}} > 1$ attraction dominates over the repulsion, the ground state gets narrower, peaked and resemble bright soliton, as shown in Fig. 3.9. This rough criterion coincides with some conclusions from the rectangular ansatz analysis. The equation (3.17) for droplets width may be written as $h(\gamma_W) = f_{\mathrm{dd}}$, with $h(\gamma) = \gamma^{-1}(2e_{\mathrm{LL}}(\gamma) - \gamma e'_{\mathrm{LL}}(\gamma))$. Importantly, the function $h(\gamma)$ fulfills $h(\gamma) < 1$ for all γ. It means that it is impossible to find a solution of (3.17) and in consequence to minimize the energy functional with the rectangular ansatz when $f_{\mathrm{dd}} > 1$. This fact suggests that the actual profile of the ground state is far from the rectangular solution.

We have to admit here that the difference between quantum droplets and solitons found in the LLGP equation is not well understood yet. Here, in fact we observe a crossover on the level of the density profile. To resolve whether we really deal with two phases with distinctive behavior one should rather inspect higher-order correlation functions. To address this problem one should use more sophisticated methods than the hydrodynamic equation studied in this thesis.

3.3. Phase transition

Finally, we give a criterion for parameters of our model, for which the stationary solution becomes localized, i.e. becomes a bright soliton or a quantum droplet. Let us start on the uniform side with stationary solution $\phi(x) = 1/\sqrt{L}$. The total energy in the presence of dipolar interactions

$$E[N, L] = \frac{N^3}{2L^2} e_{\mathrm{LL}}(\gamma) - \frac{N^2 g_{\mathrm{dd}}}{2L} \tag{3.19}$$

does not depend on the range of the dipolar interaction σ. As in the previous chapter we calculate pressure

$$P[N/L] = -\frac{\partial E[N,L]}{\partial L} = \frac{N^3}{2L^3}(2e_{\mathrm{LL}}(\gamma) - \gamma e'_{\mathrm{LL}}(\gamma)) - \frac{g_{\mathrm{dd}}N^2}{2L^2}. \tag{3.20}$$

We see that the pressure consists of two competing terms. The first one is a positive contribution from short-range repulsion, whereas the second one corresponds to negative pressure introduced by dipolar attraction. The transition occurs when the pressure crosses zero, $P[N/L] = 0$. Defining $\gamma_{\mathrm{dd}} = g_{\mathrm{dd}}L/N$ we obtain an explicit formula for the critical line

$$\gamma_{\mathrm{dd}}^{\mathrm{crit}}(\gamma) = 2e_{\mathrm{LL}}(\gamma) - \gamma e'_{\mathrm{LL}}(\gamma). \tag{3.21}$$

For $\gamma_{\mathrm{dd}} > \gamma_{\mathrm{dd}}^{\mathrm{crit}}(\gamma)$ stationary solution takes the form of a quantum droplet or bright soliton with broken translational symmetry.

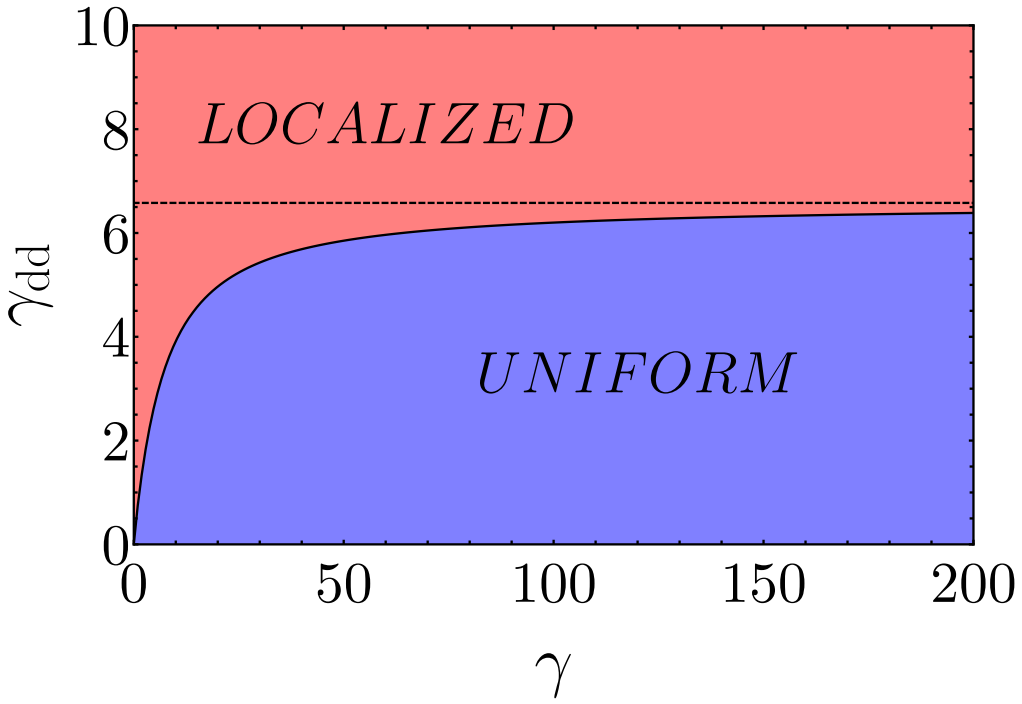

Figure 3.10: Phase diagram given by the critical line (3.21). For attraction γ_{dd} stronger than $\gamma_{\mathrm{dd}}^{\mathrm{crit}}(\infty) = \frac{2\pi^2}{3}$ (marked here with dashed line) the translational symmetry is broken regardless of the value of contact repulsion g.

Note that the condition (3.21) may be also interpreted in the picture of previously described rectangular ansatz. The equation (3.21) is exactly the minimum condition (3.17) with the droplet size equal to the ring length $W = L$. Starting from the localized phase, one may say that the transition to the uniform phase occurs, when the droplet width approaches the length of the confining ring.

The analysis presented above completes the characterization of the phases present in our model. We have to be aware of the fact that it was done with a simple hydrodynamic theory and we did not have access to higher-order correlation functions. This means that the full many-body analysis may result in a richer phase diagram. In the next chapter, we study the main subject of this thesis - elementary excitations of the dipolar gas.

Chapter 4

Elementary excitations

In this chapter we study in detail elementary excitations in different regimes. In all cases, collective modes as well as excitation energies are obtained as solutions of BdG equations. The whole procedure is similar to the one presented in Chapter 2, with a modification in the case of quantum droplets that break the translational symmetry making the analysis more complex.

4.1. Uniform phase

Let us start with the excitations of a gas with parameters from the the blue part of the phase diagram presented in Fig.3.10. We want to find the collective modes and excitation energies related to the perturbation of the uniform solution $\phi_0(x) = 1/\sqrt{L}$. We remind that the dynamics is given by the equation

$$i\frac{\partial}{\partial t}\phi = -\frac{1}{2}\frac{\partial^2\phi}{\partial x^2} + \mu_{\mathrm{LL}}\left[N|\phi|^2\right]\,\phi - g_{\mathrm{dd}}N\int dx' V^{\sigma}_{\mathrm{dd}}(x-x')|\phi(x')|^2\phi(x), \tag{4.1}$$

Here we will repeat the analysis presented in the subsection 2.2.1, but including the dipolar potential. In this case the chemical potential of the solution $\phi_0(x)$ reads

$$\mu = \mu_{\mathrm{LL}}[N/L] - \frac{g_{\mathrm{dd}}N}{L}. \tag{4.2}$$

We consider the same ansatz for time-dependent field as in the subsection 2.2.1, namely

$$\phi(x,t) = \Big(\phi_0(x) + \delta\phi(x,t)\Big)e^{-i\mu t}, \tag{4.3}$$

where the small correction to the stationary solution is assumed in the form

$$\delta\phi(x,t) = u(x)e^{-i\epsilon t} + v^*(x)e^{i\epsilon t}. \tag{4.4}$$

By applying the general form of the ansatz (4.3) into the dynamical equation (4.1) and keeping terms at most linear in $\delta\phi$ we get

$$i\partial_t\delta\phi = \Big[-\frac{1}{2}\partial_x^2 + v^2_{\mathrm{LL}}[N/L] + \mathcal{J}\Big]\delta\phi + \Big[v^2_{\mathrm{LL}}[N/L] + \mathcal{J}\Big]\delta\phi^*, \tag{4.5}$$

where we defined the following operator

$$\mathcal{J}\left[\delta\phi(x)\right] = -\frac{g_{\mathrm{dd}}N}{L}\int dx' V^{\sigma}_{\mathrm{dd}}(x-x')\delta\phi(x'). \tag{4.6}$$

Using the ansatz (4.4) for a small perturbation we obtain a pair of equations

$$\epsilon u(x) = \Big(-\frac{1}{2}\partial_x^2 + v_{\rm LL}^2[N/L] + \mathcal{J}\Big)u(x) + \Big(v_{\rm LL}^2[N/L] + \mathcal{J}\Big)v(x), \tag{4.7a}$$

$$-\epsilon v(x) = \Big(-\frac{1}{2}\partial_x^2 + v_{\rm LL}^2[N/L] + \mathcal{J}\Big)v(x) + \Big(v_{\rm LL}^2[N/L] + \mathcal{J}\Big)u(x). \tag{4.7b}$$

We are looking for solutions in the form of plane waves $u(x) = ue^{ipx}$ and $v(x) = ve^{ipx}$ with $p = 0, \pm\frac{2\pi}{L}, \pm\frac{4\pi}{L}, \ldots$ We rewrite equations (4.7a) and (4.7b)

$$\epsilon u = \Big(\frac{p^2}{2} + v_{\rm LL}^2[N/L] - \frac{g_{\rm dd}N}{L}\hat{V}_{\rm dd}^{\sigma}(p)\Big)u + \Big(v_{\rm LL}^2[N/L] - \frac{g_{\rm dd}N}{L}\hat{V}_{\rm dd}^{\sigma}(p)\Big)v, \tag{4.8a}$$

$$-\epsilon v = \Big(\frac{p^2}{2} + v_{\rm LL}^2[N/L] - \frac{g_{\rm dd}N}{L}\hat{V}_{\rm dd}^{\sigma}(p)\Big)v + \Big(v_{\rm LL}^2[N/L] - \frac{g_{\rm dd}N}{L}\hat{V}_{\rm dd}^{\sigma}(p)\Big)u, \tag{4.8b}$$

where the Fourier transform of the interaction potential $\hat{V}_{\rm dd}^{\sigma}(p) := \int dx e^{ipx} V_{\rm dd}^{\sigma}(x)$ can be calculated analytically giving

$$\hat{V}_{\rm dd}^{\sigma}(p) = 1 - F\Big(\frac{(\sigma p)^2}{2}\Big) \qquad F(x) = xe^x E_1(x), \tag{4.9}$$

where $E_1(x)$ is the exponential integral function. For small momenta $p \to 0$ the dipolar potential converges to a constant $\hat{V}_{\rm dd}^{\sigma}(p) \to 1$ and for large arguments $\hat{V}_{\rm dd}^{\sigma}(p) \sim p^{-3}$. The equations (4.8a)-(4.8b) can be easily diagonalized yielding the excitations energies

$$\epsilon(p) = \sqrt{\Big(v_{\rm LL}^2[N/L] - \frac{g_{\rm dd}N}{L}\hat{V}_{\rm dd}^{\sigma}(p)\Big)p^2 + \Big(\frac{p^2}{2}\Big)^2}. \tag{4.10}$$

Note that for large momenta $p \to \infty$ we get the dispersion relation of a free particle

$$\epsilon(p) \sim p^2/2. \tag{4.11}$$

For small momenta $p \to 0$ we recover linear phononic spectrum

$$\epsilon(p) \sim v_{\rm dd}[N/L]|p|. \tag{4.12}$$

with the speed of sound equal to $v_{\rm dd}[N/L] = \sqrt{v_{\rm LL}^2[N/L] - \frac{g_{\rm dd}N}{L}}$. Interestingly, the speed of sound may become imaginary when the dipolar attraction is sufficiently strong, and the following relation holds:

$$\frac{g_{\rm dd}N}{L} > v_{\rm LL}^2[N/L]. \tag{4.13}$$

In this case the excitation energy becomes imaginary indicating instability of the uniform solution. In order to see that imaginary excitation energy indeed implies instability we have to keep in mind the the evolution of the initial perturbation is given by factors $e^{\pm i\epsilon t}$. After sufficiently long time, the initially small perturbation will exponentially grow in time, eventually leading to a highly non-equilibrium state. The equation (4.13) may be used to find the expression for the critical value of the dipolar attraction $\gamma_{\rm dd}^{\rm cr,spec}(\gamma)$, above which the uniform solution is unstable

$$\gamma_{\rm dd}^{\rm cr,spec}(\gamma) = 3e_{\rm LL}(\gamma) - 2\gamma e'_{\rm LL}(\gamma) + \frac{1}{2}\gamma^2 e''_{\rm LL}(\gamma). \tag{4.14}$$

On the other hand, from the previous chapter we know that there is an another critical value of the dipolar attraction, given by (3.21), at which gas pressure calculated for the uniform

solution becomes negative. It is therefore crucial to compare the two expressions (3.21) and (4.14).

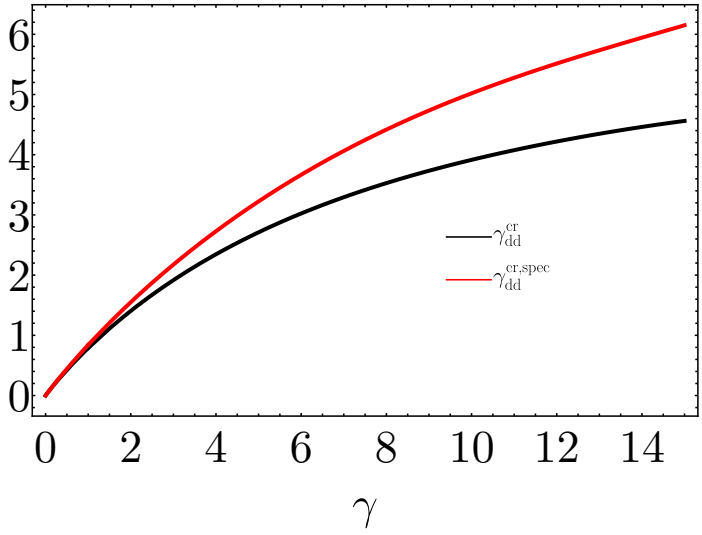

Figure 4.1: Comparison of two critical lines (3.21) and (4.14).

In Fig.4.1 we notice that for all values of contact repulsion γ it holds $\gamma_{\rm dd}^{\rm cr}(\gamma) < \gamma_{\rm dd}^{\rm cr,spec}(\gamma)$. It means that the uniform solution may be unstable, but only when it corresponds to negative pressure. On the other hand in such case we know, the the ground state solution is either a bright soliton or a quantum droplet with broken translational symmetry. Therefore, the phononic instability found here does not have any physical meaning. Before we reach the threshold (4.14) the uniform ground state solution becomes localized and we have to analyze excitations in a different way, taking modified density profile into account.

4.2. BdG equations in the non-uniform case

Here we set up the stage to analyze excitations of quantum droplets. We have to abandon the assumption that our stationary solution is uniform and this makes the analysis much more complicated. We will assume that the stationary profile $\phi_0(x)$ is real, which is the case for all stationary solutions presented before. As our profile is no longer uniform, the parameter $\gamma = gL/N$ has to be replaced with a function of position $\gamma(x) = g/N\phi_0(x)^2$. We define two auxiliary functions

$$f_1(x) = \frac{1}{2}N^2\phi_0^4(x)\Big(9e_{\rm LL}\big(\gamma(x)\big) - 5\gamma(x)e'_{\rm LL}\big(\gamma(x)\big) + \gamma^2(x)e''_{\rm LL}\big(\gamma(x)\big)\Big), \tag{4.15a}$$

$$f_2(x) = \frac{1}{2}N^2\phi_0^4(x)\Big(6e_{\rm LL}\big(\gamma(x)\big) - 4\gamma(x)e'_{\rm LL}\big(\gamma(x)\big) + \gamma^2(x)e''_{\rm LL}\big(\gamma(x)\big)\Big), \tag{4.15b}$$

and the two integral operators are defined as follows

$$\mathcal{J}_1\delta(x) = -g_{\rm dd}N\int dx' V_{\rm dd}^{\sigma}(x-x')\phi_0^2(x')\delta(x), \tag{4.16a}$$

$$\mathcal{J}_2\delta(x) = -g_{\rm dd}N\int dx' V_{\rm dd}^{\sigma}(x-x')\phi_0(x')\phi_0(x)\delta(x'). \tag{4.16b}$$

With these definitions at hand, the BdG equations in the non-uniform case may be written in a compact way

$$\epsilon u(x) = \Big(-\frac{1}{2}\partial_x^2 - \mu + f_1(x) + \mathcal{J}_1 + \mathcal{J}_2 \Big) u(x) + \Big(f_2(x) + \mathcal{J}_2 \Big) v(x), \tag{4.17a}$$

$$-\epsilon v(x) = \Big(-\frac{1}{2}\partial_x^2 - \mu + f_1(x) + \mathcal{J}_1 + \mathcal{J}_2 \Big) v(x) + \Big(f_2(x) + \mathcal{J}_2 \Big) u(x), \tag{4.17b}$$

where μ is the chemical potential of the stationary non-uniform solution $\phi_0(x)$. It is convinient to write these two equations in a matrix form

$$\begin{pmatrix} -\frac{1}{2}\partial_x^2 - \mu + f_1(x) + \mathcal{J}_1 + \mathcal{J}_2 & f_2(x) + \mathcal{J}_2 \\ -f_2(x) - \mathcal{J}_2 & \frac{1}{2}\partial_x^2 + \mu - f_1(x) - \mathcal{J}_1 - \mathcal{J}_2 \end{pmatrix} \begin{pmatrix} u \\ v \end{pmatrix} = \epsilon \begin{pmatrix} u \\ v \end{pmatrix}. \tag{4.18}$$

Following [25] we introduce a pair of new variables $r(x) := \frac{1}{2}(u(x) + v(x))$ and $s(x) := \frac{1}{2}(v(x) - u(x))$ that obey

$$\begin{pmatrix} 0 & -\frac{1}{2}\partial_x^2 - \mu + f_1(x) - f_2(x) + \mathcal{J}_1 \\ -\frac{1}{2}\partial_x^2 - \mu + f_1(x) + f_2(x) + \mathcal{J}_1 + 2\mathcal{J}_2 & 0 \end{pmatrix} \begin{pmatrix} r \\ s \end{pmatrix} = \epsilon \begin{pmatrix} r \\ s \end{pmatrix}. \tag{4.19}$$

The problem may be further simplified by acting twice with the matrix from Eq. (4.19) on the vector $[r(x),\, s(x)]^T$. This step gives two separate, seemingly independent, equations for functions $r(x)$ and $s(x)$

$$\Big(-\frac{1}{2}\partial_x^2 - \mu + f_1(x) - f_2(x) + \mathcal{J}_1 \Big) \Big(-\frac{1}{2}\partial_x^2 - \mu + f_1(x) + f_2(x) + \mathcal{J}_1 + 2\mathcal{J}_2 \Big) r(x) = \epsilon^2 r(x), \tag{4.20a}$$

$$\Big(-\frac{1}{2}\partial_x^2 - \mu + f_1(x) + f_2(x) + \mathcal{J}_1 + 2\mathcal{J}_2 \Big) \Big(-\frac{1}{2}\partial_x^2 - \mu + f_1(x) - f_2(x) + \mathcal{J}_1 \Big) s(x) = \epsilon^2 s(x). \tag{4.20b}$$

For the sake of brevity we introduce two operators

$$\hat{\mathcal{A}} := -\frac{1}{2}\partial_x^2 - \mu + f_1(x) - f_2(x) + \mathcal{J}_1, \tag{4.21a}$$

$$\hat{\mathcal{B}} := -\frac{1}{2}\partial_x^2 - \mu + f_1(x) + f_2(x) + \mathcal{J}_1 + 2\mathcal{J}_2, \tag{4.21b}$$

to cast the BdG equations in the final form

$$\hat{\mathcal{A}}\hat{\mathcal{B}} r(x) = \epsilon^2 r(x), \tag{4.22a}$$

$$\hat{\mathcal{B}}\hat{\mathcal{A}} s(x) = \epsilon^2 s(x). \tag{4.22b}$$

It is sufficient to find eigenvalues for just one equation (4.22a) or (4.22b). For instance, if $r(x)$ is an eigenvector, the corresponding eigenvector $s(x)$ of equation (4.22b) (with the same eigenvalue ϵ) may be found from (4.19). Explicitly, $s(x) = \epsilon^{-1}\hat{\mathcal{B}} r(x)$.

Eigenproblems (4.22a) and (4.22b) can be solved in the momentum space. We have to introduce momentum representation of the functions involved

$$\phi_0(x) = \frac{1}{\sqrt{L}} \sum_p \phi_p \, e^{ipx}, \tag{4.23a}$$

$$\rho(x) = \phi_0^2(x) = \frac{1}{\sqrt{L}} \sum_p \rho_p \, e^{ipx}, \tag{4.23b}$$

$$f_{1,2}(x) = \frac{1}{\sqrt{L}} \sum_p f_p^{1,2} \, e^{ipx}, \tag{4.23c}$$

as well as the matrix elements of the operators in the momentum space

$$\Big(-\frac{1}{2}\partial_x^2 \Big)_{p_1,p_2} = \frac{p_1^2}{2}\,\delta_{p_1,p_2}, \tag{4.24a}$$

$$\Big(\mu\Big)_{p_1,p_2} = \mu\delta_{p_1,p_2}, \tag{4.24b}$$

$$\Big(f_{1,2}(x)\Big)_{p_1,p_2} = f^{1,2}_{p_1-p_2}, \tag{4.24c}$$

$$\Big(\mathcal{J}_1\Big)_{p_1,p_2} = -g_{\rm dd}N\rho_{p_2-p_1}\hat{V}^{\sigma}_{\rm dd}(p_2-p_1), \tag{4.24d}$$

$$\Big(\mathcal{J}_2\Big)_{p_1,p_2} = -g_{\rm dd}N\sum_q \phi_q\phi_{p_2-p_1-q}\hat{V}^{\sigma}_{\rm dd}(q), \tag{4.24e}$$

where δ_{p_1,p_2} denotes the Kronecker delta. We use the above listed matrix elements to construct matrices $\hat{\mathcal{A}}$ and $\hat{\mathcal{B}}$ in the momentum space. Products $\hat{\mathcal{A}}\hat{\mathcal{B}}$ and $\hat{\mathcal{B}}\hat{\mathcal{A}}$ are obtained via simple matrix multiplication.

Let us note that among the solutions to the equations (4.22a) and (4.22b) there are always two zero-energy modes, similarly as in the Ref. [26] discussing excitations of two-component one-dimensional droplets. The shape of the first zero-energy solution can be easily identified and is given by the stationary solution $s(x) = \phi_0(x)$. Indeed, $\phi_0(x)$ satisfies the equation $\hat{\mathcal{A}}\phi_0(x) = 0$, hence it is an eigenvector of (4.22b) with $\epsilon = 0$.

Finally, let us touch upon the shapes of the collective modes $u(x)$ and $v(x)$. In the physical situations considered here, these functions are purely real allowing us to write down the time-dependent density profile as

$$\rho(x,t) = |\phi(x,t)|^2 \approx |\phi_0(x)|^2 + 2\phi_0(x)\Big(u(x)+v(x)\Big)\cos(\epsilon t/\hbar). \tag{4.25}$$

We see that the function $2r(x) = u(x)+v(x)$ gives the shape of the density perturbation. Note also that there is some freedom in the normalization of functions $u(x)$ and $v(x)$. This may be seen on the level of equations (4.22a) and (4.22b). These equations are clearly homogenous with respect to the functions $r(x)$ and $s(x)$. Therefore, the normalization of these functions has to be chosen and our convention for the normalization corresponds to the condition

$$\int dx\Big(|u(x)|^2 - |v(x)|^2\Big) = \frac{1}{N}. \tag{4.26}$$

Origins of a such condition may be tracked down the suggestive form of correction to the energy induced by the perturbation [15]. When the perturbation consists of different collective modes, i.e.

$$\delta\phi(x,t) = \sum_i \Big[u_i(x)e^{i\epsilon_i t} + v_i^*(x)e^{-i\epsilon_i t}\Big] \tag{4.27}$$

the energy of the perturbed state may be cast in the form $E = E_0+\delta E$, where E_0 is the energy of stationary profile $\phi_0(x)$ and δE is the energy related to the perturbation. The energy of the excited modes reads

$$\delta E = N\sum_i \int dx\Big(|u_i(x)|^2 - |v_i(x)|^2\Big)\epsilon_i. \tag{4.28}$$

Because of that form, the integral above multiplied by the particle number N is interpreted as occupation n_i of i-th excitation mode with energy ϵ_i. Our aim is to study the case of a single excited quasiparticle $n_i = 1$, hence the condition (4.29). For convenience, we may formulate the normalization condition (4.29) in terms of the function $r(x)$

$$\int dx\Big(|u(x)|^2 - |v(x)|^2\Big) = \int dx\, r(x)s(x) = \epsilon^{-1}\int dx\, r(x)\hat{\mathcal{B}}r(x) = \frac{1}{N}. \tag{4.29}$$

Technical details

The BdG equations (4.22a) and (4.22b) turned out to be challenging to solve. Solving them requires a very accurate density profile $\phi_0(x)$, which is also obtained only numerically. Since the whole method considers very small perturbation around $\phi_0(x)$, the stationary profile has to fulfill $\hat{\mathcal{A}}\phi_0(x) = 0$ to a very high accuracy. Therefore, excitations were found only in the analytical regime corresponding to fermionization limit $\gamma \to \infty$ and $\sigma \to 0$ where the energy functional simplifies to the form $e_{\mathrm{LL}}(\gamma \to \infty) = \frac{\pi^2}{3}$ and the dipolar interction potential is replaced with a delta function. The generic situation requires a more accurate method of determining the stationary solution and is left for future work, although we give some analytical approximation for excitations based on a rectangular ansatz. The initial work is done here, as we derived BdG equations for the most general case of finite γ and σ.

The stationary solution ϕ_0 is evaluated on a grid consisting of N_{grid} points. Fourier representation is found via discrete Fourier transform. Solution of the BdG equations (4.22a) and (4.22b) boils down to a diagonalization of $N_{\mathrm{grid}} \times N_{\mathrm{grid}}$ matrix. For large enough N_{grid} we observe convergence of the lowest eigenvalues and eigenvectors and occurence of two zero-energy modes.

4.3. Analysis of excitations

We consider the simplest regime of $\gamma \to \infty$ and $\sigma \to 0$, where the exact solution (3.11) is known. In this way we avoid problems related to finding numerically accurate stationary solution $\phi_0(x)$. We focus on the exemplary quantum droplet with $N = 30$ and $g_{\mathrm{dd}} = 100$. The corresponding density profile is depicted in the inset of Fig. 4.2.

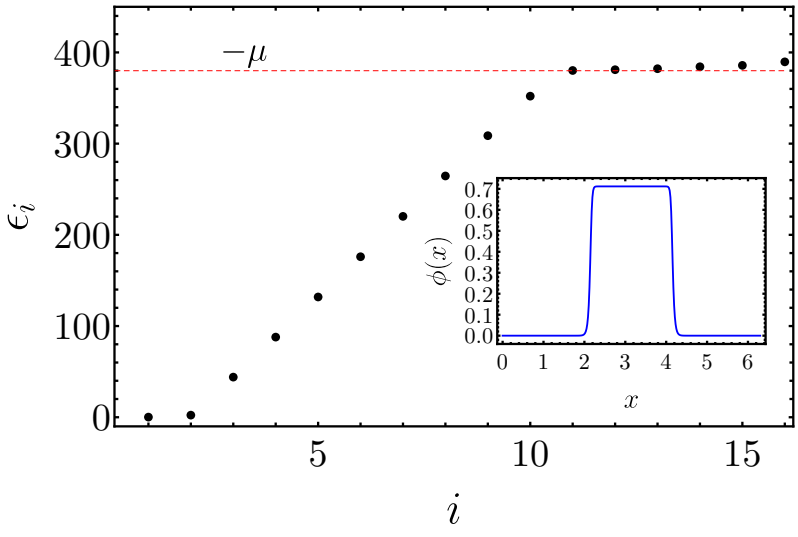

Figure 4.2: Lowest-lying excitation energies of the quantum droplet presented in the inset. The index i has no physical meaning – it enumerates the consecutive excitations.

The energies ϵ of the lowest energy excitations and shapes of the modes $r(x)$ obtained from the BdG equations are presented in Figures 4.2 and 4.3, respectively.

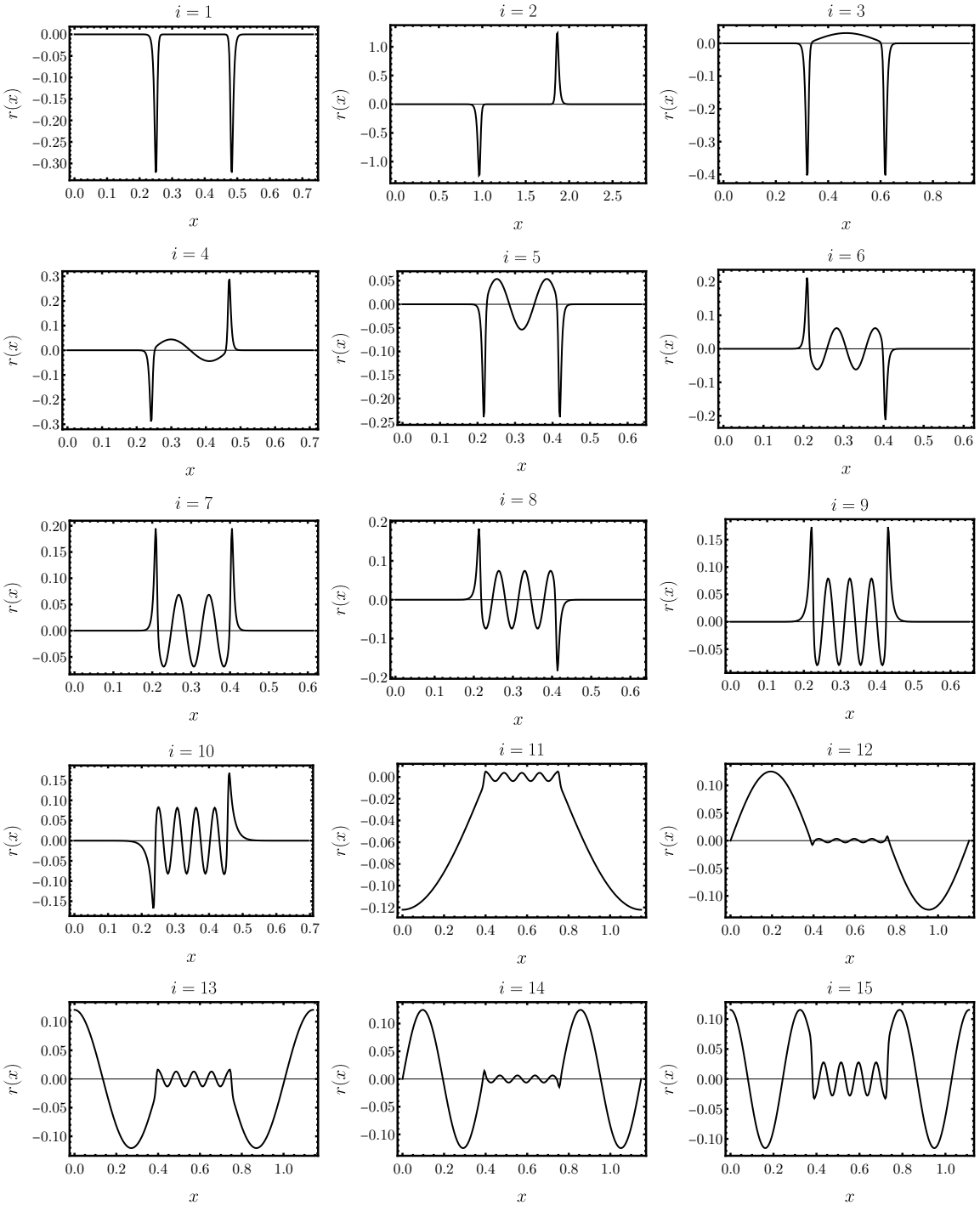

Figure 4.3: Shapes of the collective modes given by the function $r(x)$ for the droplet presented in Fig.4.2.

Firstly, let us analyze the excitation spectrum. We observe two zero-energy modes. Then, we see eight modes with energies that are linear in the mode number i. When the excitation energy reaches the absolute value of chemical potential $-\mu$, the dependence of the energy on the mode number changes drastically. These observations may be understood when looking at the shapes of excitations, presented in Fig. 4.3. In the case of the first ten modes we see

large values of function $r(x)$ for the positions corresponding to the edges of the droplet. Let us analyze further this peculiar feature. We have to keep in mind that the density perturbation is given by the formula (4.25), so the function $r(x)$ is multiplied by the density profile $\phi_0(x)$. Thus, large values of $r(x)$ are accompanied with small values of $\phi_0(x)$. Therefore, the most interesting region of function $r(x)$ is the one, where also $\phi_0(x)$ is large i.e. in the flat-top part. Here, we see that the zero-energy modes $i = 1, 2$ do not induce any non-trivial perturbation. Starting from $i = 3$ we observe cosine-like modes similar to the wavefunctions of particle in a box with a width given by the width of the droplet W. These shapes describe phononic excitations with linear dispersion visible in Fig. 4.2 (we will show later, that the linear dependence on i indeed corresponds to the linear behavior in momenta). When the energy of the phononic excitations surpasses chemical potential, the shape of exciations changes its character. We see that starting from $i = 11$ functions $r(x)$ are non-zero also outside the droplet. This implies that such excitation induces emission of the particles from the bound droplet.

Summing up, the excitations may be divided into three groups. There is a pair of zero-energy modes, that oscillate for an infinitely long time. Then there is a finite number of phononic bound modes (in this specific case we have eight such modes). Once the excitation energy goes beyond the chemical potential, the scattering modes appear, with non-zero probability density of finding a particle outside the droplet.

The results presented above were obtained from the exact numerical solution of BdG equations (4.22a) and (4.22a), written for the exact solution (3.11). However, as we see from the inset of Fig. 4.2, the density profile is not far from the rectangular solution introduced in the previous chapter. When the density profile $\phi_0(x)$ is replaced with the rectangular approximation, BdG equations can be greatly simplified. Then, the analysis strongly resembles the uniform case and the excitation spectrum is given by the formula

$$\epsilon(p) = \sqrt{\Big((\pi N/W)^2 - g_{\mathrm{dd}} N/W\Big)p^2 + \Big(\frac{p^2}{2}\Big)^2}. \tag{4.30}$$

with the allowed momenta given by the boundary conditions set by the box of width W, $p = \frac{\pi}{W}, \frac{2\pi}{W}, \ldots$. The width W may be calculated from the equation (3.17).

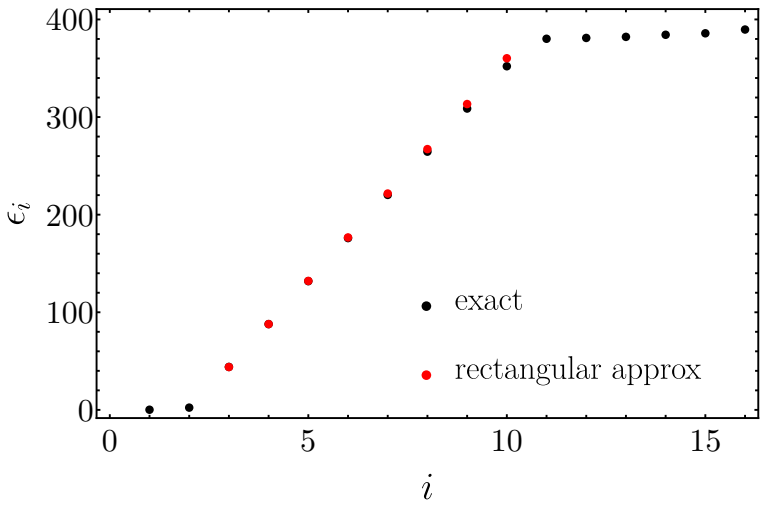

Figure 4.4: Comparison of excitation energies obtained from the full BdG equations (4.22a) and (4.22a) and the approximated results (4.30) based on the rectangular ansatz.

In Fig. 4.4 we see that the dispersion relation (4.30), based on the rectangular approximation, correctly describes energies of the bound modes, with some discrepancies near the threshold value of the excitation energy given by the absolute value of chemical potential. However, there is an infinite number of bound modes in such an approach.

We have analyzed in detail the excitations exhibited by a quantum droplet for a given value of the parameters, $N = 30$ and $g_{\mathrm{dd}} = 100$. In the remaining part of this section, we study the excitation spectrum when this two parameters of our model, N and g_{dd} are varying. Firstly, we fix $N = 30$ and study excitations of droplets between $g_{\mathrm{dd}} = 5$ and $g_{\mathrm{dd}} = 100$.

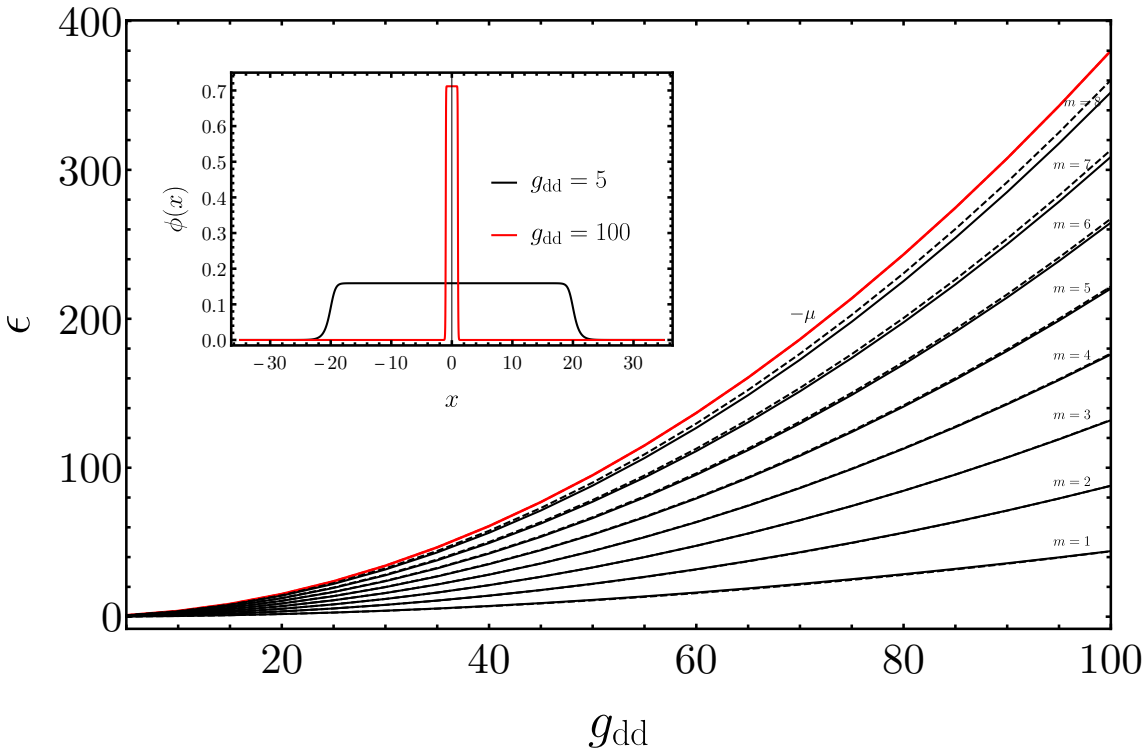

Figure 4.5: Excitation spectrum of bound modes for $N = 30$ as a function of g_{dd}. Regardless of the value of g_{dd}, the spectrum consists of eight modes with energies growing with g_{dd}. Dashed lines denote the predicitions of rectangular ansatz. Inset: density profiles for the boundary values of the considered dipolar attraction.

The results are presented in Fig. 4.5, restricted to the bound modes only. It turns out that the number of modes is independent of the parameter g_{dd}, and energies of all modes grow with the g_{dd}. Additionally, we see that rectangular ansatz works well for all considered values of the parameter g_{dd}. The differences between spectrum (4.30) marked with dashed lines and results from the exact numerical solution of BdG equations plotted with solid lines are small.

In the second scenario, we fix $g_{\mathrm{dd}} = 5$ and change the particle number from $N = 5$ to $N = 40$. The density profiles corresponding to such particle numbers are presented in Fig. 4.6. The droplet becomes wider with the growing N, consistently with the conclusions from the previous chapter. In Fig. 4.7 we show the excitation spectrum as a function of particle number N. Contrary to the previous case, the number of bound modes changes with the control parameter. As we increase N, more and more modes go below the threshold value of the excitation energy. Additionally, the energy of the modes itself is a decreasing function of N. Once again, rectangular ansatz predicitions agree well with the full solution of BdG

equations.

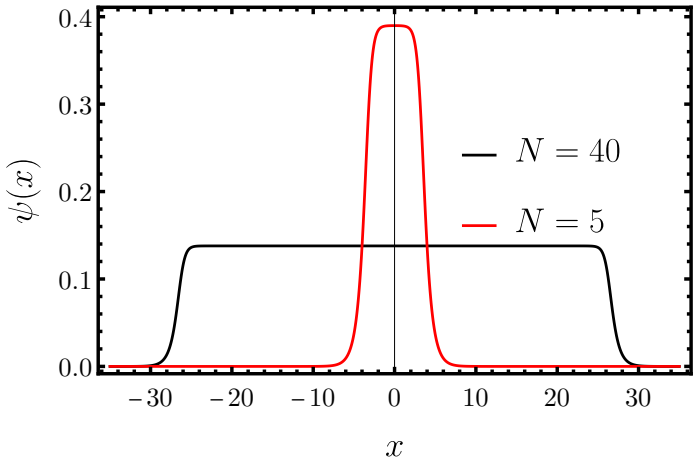

Figure 4.6: Density profiles for boundary values of considered particle numbers. The dipolar attraction is fixed at $g_{\mathrm{dd}} = 5$.

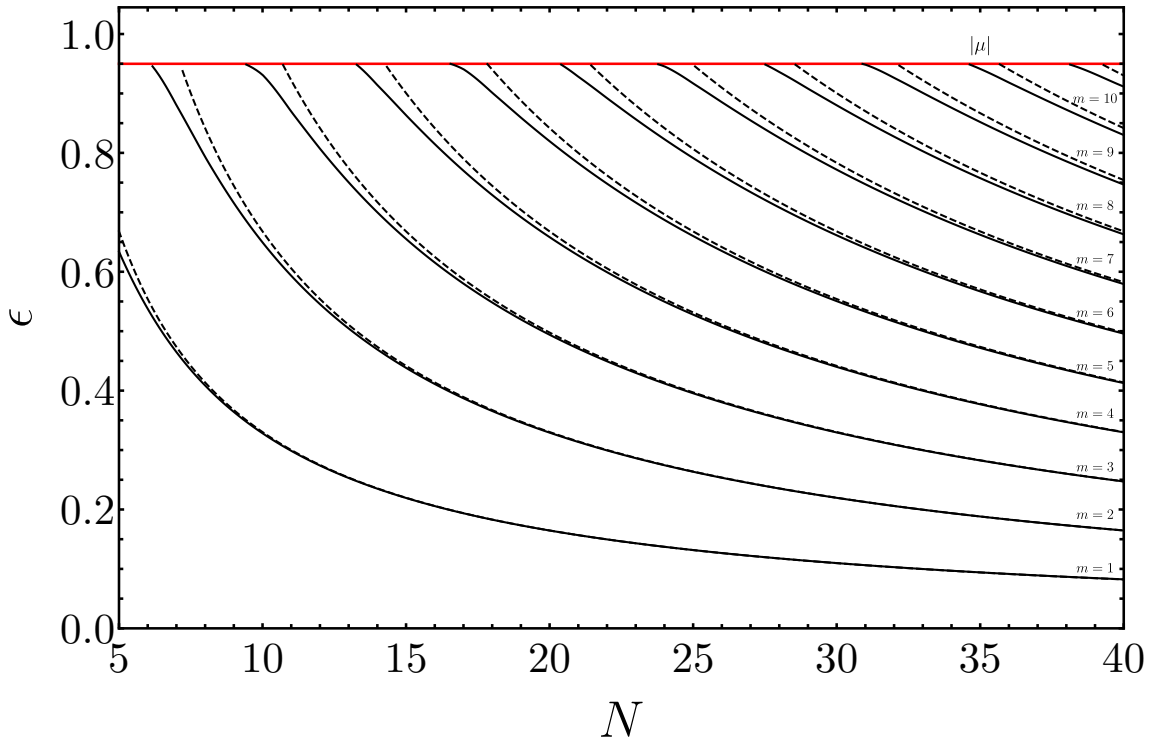

Figure 4.7: Excitation spectrum of bound modes as a function of particle number N. The dipolar attraction is fixed at $g_{\mathrm{dd}} = 5$. Dashed lines mark predicitons of rectangular ansatz.

Results presented in figures 4.4 and 4.7 raise several questions. Does the number of modes depend only on the particle number? What are the threshold values of N (for fixed g_{dd}) for which a new bound mode enters the excitation spectrum? In what manner excitation energies grow with g_{dd} and decay with N? Remarkably, all these questions may be answered analytically in the framework set by the rectangular ansatz. In the limit of fermionization,

the equation (3.17) simplifies giving width of the droplet explicitly

$$W = \frac{2\pi^2 N}{3g_{\mathrm{dd}}}. \tag{4.31}$$

Similarly, chemical potential given by (3.18) reduces to

$$\mu = -\frac{3}{8\pi^2} g_{dd}^2. \tag{4.32}$$

Excitation energy of the m-th box mode with momentum $p = \frac{m\pi}{W}$ reads

$$\epsilon_m = \frac{m}{N}\Big(\frac{3}{2\pi}\Big)^2 \sqrt{\frac{1}{3} + \frac{m^2}{4N^2}}\, g_{\mathrm{dd}}^2. \tag{4.33}$$

Hence, excitation energies grow with g_{dd} quadratically. For large N, energies decay with N as $\sim N^{-1}$. The number of bound modes is given by the condition $\epsilon_{m_{\max}} = -\mu$.

$$\frac{m_{\max}}{N}\Big(\frac{3}{2\pi}\Big)^2 \sqrt{\frac{1}{3} + \frac{m_{\max}^2}{4N^2}} = \frac{3}{8\pi^2}. \tag{4.34}$$

Note that this condition is independent of g_{dd}, in accordance with the results presented in Fig. 4.5. Moreover, the condition above gives the values of N for which a new bound mode with a number $m_{\max}$ enters the excitation spectrum. The equation above may be solved analytically leading to

$$m_{\max} = \sqrt{\frac{1}{3}(\sqrt{5} - 2)}N \approx 0.28N. \tag{4.35}$$

Hence the number of bound modes grows linearly with the particle number N. The rectangular ansatz analysis completes the characterization of excitations in the analytical regime. One may expect that such approach may also be valid for finite repulsion or non-zero σ as long as the shape of the stationary solution resembles rectangle. Below, we present excitation energies and condition for number of modes derived in such approximation. Due to previously mentioned complexity of BdG equations in these regimes, we cannot compare with full solutions and leave these results as uncertain preliminary attempts.

Excitation energies with rectangular ansatz - general case

The width W of the droplet is determined from (3.17) and the chemical potential μ is given by (3.18). The excitation energies are given by the formula

$$\epsilon_m = \sqrt{\Big(v_{\mathrm{LL}}^2[N/W] - \frac{g_{\mathrm{dd}}N}{W}\hat{V}_{\mathrm{dd}}^{\sigma}\big(\frac{m\pi}{W}\big)\Big)\big(\frac{m\pi}{W}\big)^2 + \Big(\frac{\big(\frac{m\pi}{W}\big)^2}{2}\Big)^2}. \tag{4.36}$$

The number of bound modes is determined from the transcendental equation $\epsilon_{m_{\max}} = -\mu$. It should be roughly correct as long as the stationary profile is close to a rectangular solution. We assumed here that scattering and bound modes occur not only in the analytical regime but also in generic quantum droplet solution. Although we do not have a solid argument, let us note that such structure was visible in our attempts to solve BdG equations also in different regimes. We did not manage to find satisfactory convergence of the excitation energies, but the energy of the chemical potential was clearly distinguished, dividing the modes into bound and scattering families.

Chapter 5

Summary

We demonstrated that a one-dimensional dipolar Bose gas may unravel quantum droplets and we studied their elementary excitations. A hydrodynamic theory of strongly interacting gas was constructed basing on the results from the Lieb-Liniger model. The underlying LLGP equation works for an arbitrarily strong interactions and correctly describes low-energy elementary excitations. We confirmed that observation in Chapter 2 by a direct comparison of results from linearization of LLGP equation with the exact results from the LL model.

Subsequently in the Chapter 3, we added the dipolar attraction into our model. We classified phases of the gas by dividing stationary solutions to the LLGP equation into three groups: uniform solutions, bright solitons and quantum droplets. Additionally, we found a regime where the LLGP equation is exactly solvable [24]. This is the case for infinitely strong contact repulsion and in the limit of zero range of the dipolar interactions. We have introduced an approximate rectangular ansatz that may be used to analytically predict the width of the droplet as well as its chemical potential. Lastly, we performed an analysis of phase transitions in our model. We started with a short description of bright soliton-droplet transition. In addition to that, we took a closer look at the transtion between uniform and localized stationary solutions and derived an expression for the critical line.

After that initial analysis we proceeded to study elementary excitations. This was done by the means of solving the BdG equations. For the uniform solution, we were able to derive exact expressions for excitation energies. Next, we extended our formalism to non-uniform stationary solutions and described the numerical methods. Due to the numerical complexity, we had to restrict ourselves only to the analytical regime. Here, we observed that the physically relevant modes may be divided into two groups. The first one consists of bound modes characterized by excitation energies smaller than the absolute value of the chemical potential. Such modes correspond to a small oscillations of a quantum droplet. The scattering modes, on the other hand, have excitation energies larger than the absolute value of chemical potential and display non-zero probability of finding a particle outside the droplet. Initial numerical studies suggest that such structure may be an universal feature of generic flat-top quantum droplets that are found in our model. The numerical findings were supplemented by the analytical results obtained in the rectangular ansatz approximation. A very good agreement between these two methods was observed. Additionally, we presented results for excitations based on the rectangular ansatz also outside the analytically solvable regime. However, the full solution of BdG equations in a generic regime still awaits more accurate method of finding the stationary solution. This is left for future work.

Appendix A

Imaginary time evolution method

The stationary solutions presented in this thesis are solutions of complex, nonlinear equation (3.7). Given the complicted form of $e_{\mathrm{LL}}(\gamma)$ and the non-local character of dipolar interactions, the equation cannot be solved analytically in the general case. One has to look for approximate, numerical method. Throughout this work, we will always use the so-called imaginary time evolution (ITE) method, working as follows.

We discretize the space into N_{grid} points with grid spacing Δx. The starting point of the algorithm corresponds to proposition of a initial, trial function $\phi(x)$. Then, we "evolve" this initial function in the imaginary time $t \to -i\tau$ applying the "evolution" operator $e^{-H\tau}$ in a consecutive, small steps. Here, H denotes the energy functional (3.6). After the each step, the resulting, new density profile is normalized. Algorithm ends when the relative differences between energies of the profiles obtained in consecutive steps are smaller than some very small, fixed number.

In this thesis I was using the implementation of the algorithm availible here `https://gitlab.com/jakkop/mudge/-/tags/v01Jun2021`. I did not contribute to the code in any form.

Appendix B

Accurate representation of the function $e_{LL}(\gamma)$

The LLGP equation assumes explicit knowledge of the function $e_{\rm LL}(\gamma)$ introduced in [12]. Fortunately, there are an extremely accurate approximations for that function in the whole region of the interaction strength γ. Here, we write down the results of [27]. For the weakly interacting gas $\gamma < 1$ we have

$$e_{\rm LL}(\gamma) = \gamma - \frac{4}{3\pi}\gamma^{3/2} + \left[\frac{1}{6} - \frac{1}{\pi^2}\right]\gamma^2 - 0.0016\gamma^{5/2} + O(\gamma^3). \tag{B.1}$$

In the regime of intermediate interactions $1 \leq \gamma < 15$ the approximation reads

$$e_{\rm LL}(\gamma) \approx \gamma - \frac{4}{3\pi}\gamma^{3/2} + \left[\frac{1}{6} - \frac{1}{\pi^2}\right]\gamma^2 - 0.002005\gamma^{5/2} + 0.000419\gamma^3 - 0.000284\gamma^{7/2} + 0.000031\gamma^4. \tag{B.2}$$

Finally, nearly TG regime $\gamma \geq 15$ we have the following

$$\begin{aligned} e_{\rm LL}(\gamma) \approx \frac{\pi^2}{3}\Bigg(1 - \frac{4}{\gamma} + \frac{12}{\gamma^2} - \frac{10.9448}{\gamma^3} - \frac{130.552}{\gamma^4} + \frac{804.13}{\gamma^5} - \frac{910.345}{\gamma^6} - \frac{15423.8}{\gamma^7} + \\ \frac{100559.}{\gamma^8} - \frac{67110.5}{\gamma^9} - \frac{2.64681\times 10^6}{\gamma^{10}} + \frac{1.55627\times 10^7}{\gamma^{11}} + \frac{4.69185\times 10^6}{\gamma^{12}} - \\ \frac{5.35057\times 10^8}{\gamma^{13}} + \frac{2.6096\times 10^9}{\gamma^{14}} + \frac{4.84076\times 10^9}{\gamma^{15}} - \frac{1.16548\times 10^{11}}{\gamma^{16}} + \\ \frac{4.35667\times 10^{11}}{\gamma^{17}} + \frac{1.93421\times 10^{12}}{\gamma^{18}} - \frac{2.60894\times 10^{13}}{\gamma^{19}} + \frac{6.51416\times 10^{13}}{\gamma^{20}} + O\left(\frac{1}{\gamma^{21}}\right)\Bigg). \end{aligned} \tag{B.3}$$

The results presented in Chapter 2 are published in a preprint:

1. J. Kopyciński, M. Łebek, M. Marciniak, R. Ołdziejewski, W. Górecki, K. Pawłowski, *Beyond Gross-Pitaevskii equation for 1D gas: quasiparticles and solitons*, arXiv:2106.15289 (2021)

The results of Chapters 3 and 4 are planned to be published in the near future.

List of publications and preprints beyond the scope of this thesis:

2. M. Łebek, A. Syrwid, P. T. Grochowski, K. Rzążewski, *Repulsive dynamics of strongly attractive one-dimensional quantum gases*, arXiv:2107.05594 (2021)

3. A. Syrwid, M. Łebek, P. T. Grochowski, K. Rzążewski, *Many-body molecule formation at a domain wall in a one-dimensional strongly interacting ultracold Fermi gas*, arXiv:2105.00439 (2021)

4. M. Łebek, P. Jakubczyk, *Thermodynamic Casimir forces in strongly anisotropic systems within the $N \to \infty$ class*, SciPost Phys. Core 4, 016 (2021)

5. M. Łebek, P. T. Grochowski, K. Rzążewski, *Single- to many-body crossover of a quantum carpet* , Phys. Rev. Research 3, 023009 (2021)

6. M. Łebek, P. Jakubczyk, *Dimensional crossovers and Casimir forces for the Bose gas in anisotropic optical lattices* , Phys. Rev. A 102, 013324 (2020)

7. M. Kruk, M.Łebek, K. Rzążewski, *Statistical properties of cold bosons in a ring trap* , Phys. Rev. A 101, 023622 (2020)

Bibliography

[1] M. H. Anderson, J. R. Ensher, M. R. Matthews, C. E. Wieman, and E. A. Cornell. Observation of Bose-Einstein condensation in a dilute atomic vapor. *Science (80-.).*, 269(5221):198–201, jul 1995.

[2] K. B. Davis, M. O. Mewes, M. R. Andrews, N. J. Van Druten, D. S. Durfee, D. M. Kurn, and W. Ketterle. Bose-Einstein condensation in a gas of sodium atoms. *Phys. Rev. Lett.*, 75(22):3969–3973, nov 1995.

[3] M. R. Andrews, C. G. Townsend, H.-J. Miesner, D. S. Durfee, D. M. Kurn, and W. Ketterle. Observation of Interference Between Two Bose Condensates. *Science (80-.).*, 275(5300):637–641, jan 1997.

[4] Holger Kadau, Matthias Schmitt, Matthias Wenzel, Clarissa Wink, Thomas Maier, Igor Ferrier-Barbut, and Tilman Pfau. Observing the Rosensweig instability of a quantum ferrofluid. *Nature*, 530(7589):194–197, feb 2016.

[5] D. S. Petrov. Quantum Mechanical Stabilization of a Collapsing Bose-Bose Mixture. *Phys. Rev. Lett.*, 115(15):155302, oct 2015.

[6] T. D. Lee, Kerson Huang, and C. N. Yang. Eigenvalues and eigenfunctions of a Bose system of hard spheres and its low-temperature properties. *Phys. Rev.*, 106(6):1135–1145, jun 1957.

[7] C. R. Cabrera, L. Tanzi, J. Sanz, B. Naylor, P. Thomas, P. Cheiney, and L. Tarrue. Quantum liquid droplets in a mixture of bose-Einstein condensates. *Science (80-.).*, 359(6373):301–304, jan 2018.

[8] D. S. Petrov and G. E. Astrakharchik. Ultradilute Low-Dimensional Liquids. *Phys. Rev. Lett.*, 117(10):100401, sep 2016.

[9] Abdelâali Boudjemâa. Two-dimensional quantum droplets in dipolar Bose gases. *New J. Phys.*, 21(9):093027, sep 2019.

[10] Ivan Morera, Grigori E. Astrakharchik, Artur Polls, and Bruno Juliá-Díaz. Universal Dimerized Quantum Droplets in a One-Dimensional Lattice. *Phys. Rev. Lett.*, 126(2):023001, jan 2021.

[11] Rafał Ołdziejewski, Wojciech Górecki, Krzysztof Pawłowski, and Kazimierz Rzążewski. Strongly Correlated Quantum Droplets in Quasi-1D Dipolar Bose Gas. *Phys. Rev. Lett.*, 124(9):090401, mar 2020.

[12] Elliott H. Lieb. Exact analysis of an interacting bose gas. II. the excitation spectrum. *Phys. Rev.*, 130(4):1616–1624, may 1963.

[13] Elliott H. Lieb and Werner Liniger. Exact analysis of an interacting bose gas. I. the general solution and the ground state. *Phys. Rev.*, 130(4):1605–1616, may 1963.

[14] Franco Dalfovo, Stefano Giorgini, Lev P. Pitaevskii, and Sandro Stringari. Theory of Bose-Einstein condensation in trapped gases. *Rev. Mod. Phys.*, 71(3):463, apr 1999.

[15] L. P. Pitaevskii and S. Stringari. *Bose-Einstein Condensation*. International Series of Monographs on Physics. Clarendon Press, 2003.

[16] M. Girardeau. Relationship between Systems of Impenetrable Bosons and Fermions in One Dimension. *J. Math. Phys.*, 1(6):516, dec 2004.

[17] Bogdan Damski. Formation of shock waves in a Bose-Einstein condensate. *Phys. Rev. A*, 69(4):043610, apr 2004.

[18] S. Choi, V. Dunjko, Z.D. Zhang, and M. Olshanii. Monopole Excitations of a Harmonically Trapped One-Dimensional Bose Gas from the Ideal Gas to the Tonks-Girardeau Regime. *Phys. Rev. Lett.*, 115(11):115302, sep 2015.

[19] Sebastiano Peotta and Massimiliano Di Ventra. Quantum shock waves and population inversion in collisions of ultracold atomic clouds. *Phys. Rev. A*, 89(1):013621, jan 2014.

[20] Eugene B. Kolomeisky, T. J. Newman, Joseph P. Straley, and Xiaoya Qi. Low-Dimensional Bose Liquids: Beyond the Gross-Pitaevskii Approximation. *Phys. Rev. Lett.*, 85(6):1146, aug 2000.

[21] M. D. Girardeau and E. M. Wright. Breakdown of Time-Dependent Mean-Field Theory for a One-Dimensional Condensate of Impenetrable Bosons. *Phys. Rev. Lett.*, 84(23):5239, jun 2000.

[22] Zoran Ristivojevic. Excitation Spectrum of the Lieb-Liniger Model. *Phys. Rev. Lett.*, 113(1):015301, jul 2014.

[23] F. Deuretzbacher, J. C. Cremon, and S. M. Reimann. Ground-state properties of few dipolar bosons in a quasi-one-dimensional harmonic trap. *Phys. Rev. A*, 81(6):063616, jun 2010.

[24] B B Baizakov, F Kh Abdullaev, B A Malomed, and M Salerno. Solitons in the Tonks–Girardeau gas with dipolar interactions. *J. Phys. B At. Mol. Opt. Phys.*, 42(17):175302, aug 2009.

[25] Shai Ronen, Daniele C. E. Bortolotti, and John L. Bohn. Bogoliubov modes of a dipolar condensate in a cylindrical trap. *Phys. Rev. A*, 74(1):013623, jul 2006.

[26] Marek Tylutki, Grigori E. Astrakharchik, Boris A. Malomed, and Dmitry S. Petrov. Collective excitations of a one-dimensional quantum droplet. *Phys. Rev. A*, 101(5):051601, may 2020.

[27] Guillaume Lang, Frank Hekking, and Anna Minguzzi. Ground-state energy and excitation spectrum of the Lieb-Liniger model : accurate analytical results and conjectures about the exact solution. *SciPost Phys.*, 3(1):003, jul 2017.